



# A Conceptual Model of Polar Overturning Circulations

Thomas W. N. Haine\*

*Earth & Planetary Sciences, Johns Hopkins University, Baltimore, Maryland*

\**Corresponding author:* Thomas W. N. Haine, [Thomas.Haine@jhu.edu](mailto:Thomas.Haine@jhu.edu)

1

**Early Online Release:** This preliminary version has been accepted for publication in *Journal of the Physical Oceanography*, may be fully cited, and has been assigned DOI 10.1175/JPO-D-20-0139.1. The final typeset copyedited article will replace the EOR at the above DOI when it is published.

## ABSTRACT

The global ocean overturning circulation carries warm, salty water to high latitudes, both in the Arctic and Antarctic. Interaction with the atmosphere transforms this inflow into three distinct products: sea ice, surface Polar Water, and deep Overflow Water. The Polar Water and Overflow Water form estuarine and thermal overturning cells, stratified by salinity and temperature, respectively. A conceptual model specifies the characteristics of these water masses and cells given the inflow and air/sea/land fluxes of heat and freshwater. The model includes budgets of mass, salt, and heat, and parametrizations of Polar Water and Overflow Water formation, which include exchange with continental shelves. Model solutions are mainly controlled by a linear combination of air/sea/ice heat and freshwater fluxes and inflow heat flux that approximates the meteoric freshwater flux plus the sea ice export flux. The model shows that for the Arctic, the thermal overturning is likely robust, but the estuarine cell appears vulnerable to collapse via a so-called heat crisis that violates the budget equations. The system is pushed towards this crisis by increasing Atlantic Water inflow heat flux, increasing meteoric freshwater flux, and/or decreasing heat loss to the atmosphere. The Antarctic appears close to a so-called Overflow Water emergency with weak constraints on the strengths of the estuarine and thermal cells, uncertain sensitivity to parameters, and possibility of collapse of the thermal cell.

## 1. Introduction

The global ocean overturning circulation is transformed in the high latitudes of both hemispheres. The transformation is achieved by extraction of heat to the atmosphere, addition of meteoric freshwater (from precipitation minus evaporation, river runoff, and iceberg calving), and interaction with ice. Understanding how warm salty inflows to polar oceans partition into different outflow components is primitive, however, and this question is important for oceanography and climate science. To address it, this paper presents and explores a conceptual physical model and applies it to both the Arctic and the Antarctic.

The Arctic Ocean and Nordic Seas are separated from the global ocean by relatively shallow ridges between Greenland and Scotland. The flow across these ridges consists of surface-intensified warm salty water from the North Atlantic Current flowing north (Hansen et al. 2008). Returning south are three distinct water types (Hansen and Østerhus 2000; Østerhus et al. 2005). First, there is overflow water, which spills into the North Atlantic Ocean through gaps in the ridges. Overflow water is cooler and denser than the inflow, but of similar salinity. Second, there is a cold fresh surface outflow in the East Greenland Current (Rudels et al. 2002). The East Greenland Current also carries the third water type, which is sea ice.

The exchange between the Nordic Seas and the Arctic Ocean across the Fram Strait and Barents Sea Opening is essentially the same. Fig. 1 shows the hydrographic characteristics and currents. The warm salty inflow is Atlantic Water (AW), which flows north in the eastern halves of the Barents Sea Opening and the Fram Strait. The net AW flux into the Arctic is about 4 Sv (Tsubouchi et al. 2012, 2018; some also recirculates in Fram Strait; 1 Sv equals  $10^6\text{m}^3\text{s}^{-1}$ ). The AW temperature exceeds about  $3^\circ\text{C}$  with a salinity around 35.00 g/kg and a seasonal cycle that leads to summer surface freshening and warming (Fig. 1 lower panel). The three outflows are Overflow Water

(OW), which is cooler and denser than AW, but of similar salinity (the closest water type from Tsubouchi et al. (2018) is their Intermediate Water, but we adopt OW here, consistent with Eldevik and Nilsen 2013). OW leaves the Arctic on the western side of Fram Strait in the deep part of the East Greenland Current. Above OW is Polar Water (PW), which is near the freezing temperature and fresher than AW (Tsubouchi et al. 2018 call this Surface Water). As for AW, the PW is warmer and fresher in summer. Sea ice occupies the western part of Fram Strait and the East Greenland continental shelf, flowing in the East Greenland Current. The split between OW and PW transport is about 3:1 across Fram Strait and the Barents Sea Opening (this estimate, from Tsubouchi et al. 2018 Fig. 4, is representative not precise, due mainly to the non-zero flow across Fram Strait and the Barents Sea Opening). The sea ice flux is about 0.064 Sv (Haine et al. 2015).

The Antarctic meridional overturning circulation is essentially similar. The inflow of warm salty water occurs in Circumpolar Deep Water (CDW), analogous to AW (it is called AW below), and fed from the deep North Atlantic. CDW upwells towards the surface beneath the Antarctic Circumpolar Current (Marshall and Speer 2012; Talley 2013). Air/sea/ice interaction around Antarctica transforms the CDW in two meridional overturning cells that circulate back north. The upper cell is stronger with a transport of about 22 Sv, equivalent to 80% of the CDW flux (Abernathey et al. 2016; Pellichero et al. 2018). This cell feeds fresh, cold surface water that is called Winter Water when the summer thermal stratification is removed. It is analogous to Arctic PW. The Winter Water flows north and subducts as Subantarctic Mode Water (SAMW) and Antarctic Intermediate Water (AAIW), which are less dense than CDW mainly because they are fresher. SAMW and AAIW form in deep winter mixed layers near the Subantarctic Front, with several processes involved and substantial zonal flow (McCartney 1977; Cerovečki et al. 2013; Gao et al. 2017). Associated with Winter Water is sea ice, which forms primarily near Antarctica in winter and flows north with a flux that is estimated to be 0.13 Sv (Haumann et al. 2016) and 0.36 Sv

(Abernathy et al. 2016). The lower cell produces Antarctic Bottom Water (AABW) from CDW by cooling, freezing, and salinification, especially on the continental shelves in the Weddell and Ross Seas and around east Antarctica (Foster and Carmack 1976; Orsi et al. 1999; Jacobs 2004). AABW is analogous to Arctic OW. The resulting dense, saline, freezing shelf water overflows the shelf break into the deep ocean. As it descends, the dense plume entrains and mixes with ambient CDW to form AABW (Muench et al. 2009; Naveira Garabato et al. 2002).

To our knowledge, no prior study quantifies both estuarine and thermal overturning cells in the Arctic and Antarctic. Nevertheless, the key ideas in the present model are well known in the polar oceanography literature. First, consider the salinization process to produce dense shelf water: Gill (1973) argues that brine release during winter freezing on the continental shelves of the Weddell Sea produces dense saline water that overflows the shelf break to form AABW. He points to the wind driven export of sea ice offshore to maintain high freezing rates in coastal polynyas. This process is corroborated using Arctic satellite microwave data by Tamura and Ohshima (2011). Aagaard et al. (1981) describe the maintenance of the Arctic halocline by salinization of shelf water in winter by freezing and export of sea ice. Their observations show freezing shelf water with high salinity, in some cases 2–4 g/kg higher than in summer. Extending this work, Aagaard et al. (1985) propose that a major source of Arctic deep water is dense brine-enriched shelf water. Quadfasel et al. (1988) present observational evidence of the shelf overflow and entrainment process occurring in Storfjorden, Svalbard. They observe shelf water with salinities of about 35.5 g/kg (about 0.5 g/kg saltier than the AW in Fram Strait) at the freezing temperature (see also Maus 2003). Rudels and Quadfasel (1991) review the importance of dense shelf water overflow for the deep Arctic Ocean thermohaline structure. They conclude that it must dominate open-ocean deep convection, although this latter process occurs variably in the Greenland Sea. Freezing and brine rejection drive both deep convection and shelf overflows in their view, consistent with Aagaard et al. (1985).

More recently, Rudels (2010, 2012) articulates the problem of understanding Arctic water mass transformation and the Arctic estuarine and thermal overturning cells together (he refers to them as a “double estuary”). His papers address several issues that underpin the present work: formation of the fresh PW layer, conversion of AW to PW, separation between the estuarine and thermal cells, formation of deep water, and exchange through Fram Strait. Abernathey et al. (2016) and Pellichero et al. (2018) also view the Antarctic system in an holistic way. They focus on the upper estuarine cell and the importance of sea ice in moving freshwater from the shelves to freshen SAMW and AAIW. Eldevik and Nilsen (2013) define the problem of quantifying the two Arctic overturning cells (they refer to them as the “Arctic-Atlantic thermohaline circulation”). Their model consists of volume, salinity, and heat budgets, similar to eq. (1) below. However, to close their problem and solve for the outflow transports they must specify the temperature and salinity properties of PW and OW. They also neglect sea ice. Therefore, their system is a special case of the model presented here, which does not make these assumptions.

This paper synthesizes these ideas. It builds, explains, and applies a quantitative model of polar overturning circulation. The model is conceptual so as to elucidate principles and characteristics. It neglects many important effects including seasonality, interannual variability, regional differences, and continuously varying hydrographic properties. It includes budgets for mass, salt, and heat and physical parametrizations of PW and OW formation. Although it respects physical principles, the model is essentially kinematic. The dynamics of the overturning circulations are beyond the model’s scope, and likely differ between the Arctic and Antarctic. Nevertheless, the dynamics must in aggregate respect the budget and parametrization equations used here.

## 2. Conceptual Model

Consider the system sketched in Fig. 2 (top panel): A deep polar basin is fed across a gateway from lower latitudes with relatively warm, salty Atlantic Water (AW). The polar basin connects to a shallow polar continental shelf across a shelf break. The basin and shelf exchange heat and freshwater with the atmosphere. The basin returns three distinct water classes to lower latitudes (see Fig. 3 for a temperature/salinity schematic), namely: Overflow Water (OW), which is a cooled, denser version of AW, with similar salinity; Polar Water (PW), which is a fresh, freezing, less dense version of AW; and, sea ice. Sea ice formation (freezing) occurs on the shelf and there is partial sea ice melting in the basin. The AW to OW pathway comprises the thermal overturning cell and the AW to PW plus sea ice comprises the estuarine overturning cell. Fig. 2 (bottom panel) shows the model parameters, principles, and output variables.

The model specifies steady seawater mass, salt, and heat budgets for two control volumes: the basin sea ice melting region and the continental shelf sea ice freezing region (following Eldevik and Nilsen 2013). In the **basin**:

$$\begin{aligned}
 \sum_{j=1,2,3,i} \rho_j U_j - \sum_{j=1,i,s} \rho_j u_j &= \mathcal{F}_b && \text{mass conservation,} \\
 \sum_{j=1,2,3,i} \rho_j U_j S_j - \sum_{j=1,i,s} \rho_j u_j S_j &= 0 && \text{salt conservation,} \\
 c_p \sum_{j=1,2,3} \rho_j U_j T_j - c_p \sum_{j=1,s} \rho_j u_j T_j - \rho_i L' (U_i - u_i) &= \mathcal{Q}_b && \text{heat conservation.} \quad (1)
 \end{aligned}$$

Notation is in Table 1. The volume fluxes (transports) are  $U_j$  and  $u_j$ , temperatures are  $T_j$ , and salinities are  $S_j$  (the associated density is  $\rho_j = \rho(T_j, S_j)$ ). The subscripts correspond to: 1 = Atlantic Water (AW), 2 = Polar Water (PW), 3 = Overflow Water (OW), i = sea ice, s = Shelf Water (SW). The surface ocean freshwater mass and heat flux parameters are  $\mathcal{F}_b$  and  $\mathcal{Q}_b$ , respectively.

Inflowing freshwater is assumed to have a temperature of 0°C and the heat budget is relative to 0°C. The sign conventions are:

- Positive volume fluxes  $U_j$  mean poleward flow. So  $U_1$  is positive and all the others are negative.
- Positive fluxes  $\mathcal{F}_b$ ,  $Q_b$  mean ocean to atmosphere freshwater and heat fluxes (i.e., ocean salinifying and cooling). So  $\mathcal{F}_b$  is negative and  $Q_b$  is positive.

Assume that not all the sea ice melts,  $U_i < 0$ , and therefore  $T_2 = T_f$ , where  $T_f$  is the freezing temperature (evaluated at the appropriate salinity). Finally,  $L' = L - c_p T_f + c_i (T_f - T_i)$ ,  $L$  is the latent heat of freezing for seawater,  $T_i$  is sea ice temperature, and  $c_p, c_i$  are the specific heat capacities of seawater and sea ice, respectively.

Similarly, on the **shelf**:

$$\begin{aligned}
 \sum_{j=1,i,s} \rho_j u_j &= \mathcal{F}_s && \text{mass conservation,} \\
 \sum_{j=1,i,s} \rho_j u_j S_j &= 0 && \text{salt conservation,} \\
 c_p \sum_{j=1,s} \rho_j u_j T_j - \rho_i L' u_i &= Q_s && \text{heat conservation.} \tag{2}
 \end{aligned}$$

Assume that SW forms from AW by cooling and freshwater input (with no PW contribution). The products are SW with properties  $T_s, S_s$  and sea ice that leaves the shelf for the basin. Freezing requires that  $u_i < 0$  and therefore  $T_s = T_f$ . We specify the AW properties  $T_1, S_1, U_1$  and the surface fluxes for basin and shelf together,  $Q = Q_b + Q_s, \mathcal{F} = \mathcal{F}_b + \mathcal{F}_s$ . The unknowns are the SW, OW, PW, and sea ice properties, so further assumptions are necessary to close (1) and (2).

Assume that PW is formed from AW by heat loss to the atmosphere and to melt sea ice (following Klinger and Haine 2019, Chapter 10; Rudels 2016; Abernathey et al. 2016; Pellichero et al. 2018, and Fig. 3). The AW is cooled to freezing temperature and freshened by melt. In order to maintain



the stably stratified PW layer above the AW layer, we require that  $\rho_2 < \rho_1$ . This sets the maximum allowed PW salinity given the AW inflow properties:

$$S_2 \leq \frac{\beta(S_1 - S_i)(L' + c_p T_f) S_1 + \alpha(T_1 - T_f)(L' + c_p T_1) S_i}{\beta(S_1 - S_i)(L' + c_p T_f) + \alpha(T_1 - T_f)(L' + c_p T_1)} \quad \text{static stability,} \quad (3)$$

where  $\alpha$  and  $\beta$  are the thermal expansion and haline contraction coefficients (evaluated for the TEOS-10 equation of state at the AW temperature and salinity). This formula expresses linear mixing between  $S_1$  and  $S_i$ . The PW properties lie at the intersection of the freezing temperature and the line tangent to the isopycnal at the AW properties: see Fig. 3. This ensures that as PW is formed from AW by cooling and freshening it always remains less dense than AW. In any case,  $S_2$  is treated as a parameter that varies in section 3f.

Assume that OW is formed from SW and a mixture of AW and PW that is entrained during the overflow. The influential Price and O'Neil Baringer (1994) model is used for this process (their end-point model, not the streamtube model: see also discussion in section 4). It computes the OW product properties of the plume descending from a marginal sea and entraining ambient water (aW). It assumes the plume is geostrophic and the bottom stress causes the plume to grow downstream in width due to Ekman drainage. Entrainment of aW (and mixing with it) occurs at hydraulic jumps as determined by a geostrophic Froude number  $F_{\text{geo}}$ . The entrainment strength  $\Phi$  depends on  $F_{\text{geo}}$  and specifies the aW/SW mixing to form OW. The Froude number is proportional to the overflow plume speed and inversely proportional to the (square root of) plume thickness. The plume thickness and speed depend on the plume flux and the plume width, and the plume width increases downstream. The net effect of these factors is that entrainment decreases (weakly) as the SW flux increases and entrainment increases as the aW/SW density difference increases.

Specifically, linear mixing implies

$$T_3 = \Phi T_a + (1 - \Phi) T_f \quad \text{heat conservation,} \quad (4)$$

$$S_3 = \Phi S_a + (1 - \Phi) S_s \quad \text{salt conservation,} \quad (5)$$

where  $(T_f, S_s)$  are the SW properties and  $(T_a, S_a)$  are the aW properties (i.e., the water that is entrained: see Fig. 3). The entrainment parameter  $0 \leq \Phi \leq 1$  is the mass fraction that determines the mixing between aW and SW to form OW:

$$\Phi = 1 - \frac{\rho_s u_s}{\rho_3 U_3} \quad \text{mixing mass fraction.} \quad (6)$$

Price and O'Neil Baringer (1994) parametrize the entrainment as

$$\Phi = \max\left(0, 1 - F_{\text{geo}}^{-2/3}\right) \quad (7)$$

for geostrophic Froude number

$$F_{\text{geo}} = \frac{g(\rho_s - \rho_a) \alpha_{\text{max}}^{3/2} (W_s + 2K_{\text{geo}} x)^{1/2}}{\rho_0 f^{3/2} u_s^{1/2}}. \quad (8)$$

Thus,

$$\Phi = \max\left(0, 1 - \gamma \frac{|u_s|^{1/3}}{(\rho_s - \rho_a)^{2/3}}\right) \quad \text{plume entrainment model,} \quad (9)$$

where  $\gamma = \rho_0^{2/3} f g^{-2/3} \alpha_{\text{max}}^{-1} (W_s + 2K_{\text{geo}} x)^{-1/3}$  is a constant and the parameters have conventional meanings (see Table 1 and section 3g).

Additionally, the aW properties (entrained into the plume) are set by a mixing mass fraction,  $0 \leq \phi \leq 1$ , between surface PW and AW:

$$T_a = \phi T_f + (1 - \phi) T_1 \quad \text{heat conservation,} \quad (10)$$

$$S_a = \phi S_2 + (1 - \phi) S_1 \quad \text{salt conservation,} \quad (11)$$

(see Fig. 3). Observations show the OW is cooler and fresher than AW indicating  $\phi > 0$  (Fig. 1, this is also true in the Antarctic case: see Fig. 3 in Nicholls et al. 2009). The mixture fraction  $\phi$  is formally another parameter in the conceptual model. It is constrained, however, and it is initially held fixed (see supplement section S4).

#### *a. Model Solution*

The full system consists of equations for mass, salt, and heat conservation (1), (2); linear mixing (4), (5), (10), (11); and plume entrainment (6), (9). Inequalities enforce static stability with the densities ordered from SW (densest) to OW to AW to PW (least dense). Inequalities also enforce physically-relevant solutions, namely, sign constraints on the transports. This is a system of six equations in six unknowns, namely,  $\{U_2, U_3, U_i, u_1, u_i, S_s\}$  (see also supplement section S1). There are five flux parameters:  $\{U_1, U_1 T_1, U_1 S_1, Q, \mathcal{F}\}$ , and the overflow mixing fraction  $\phi$ .

The model consists of coupled nonlinear algebraic equations. The most important nonlinearity is due to the parametrization of entrainment (6) and (9), although there are several others due to the advective product of variables and seawater functions of state. Therefore, we expect multiple solutions, possibly an infinite number, for some parameter ranges, and no solutions for others. For the case of an infinite number of solutions we expect tradeoffs between variables and bounds on variables within limits. One goal is to diagnose and understand these different types of solution. The system is solved iteratively using a procedure explained in supplement section S1. Solutions satisfy the equations exactly except for (9), which is satisfied within a tolerance  $\delta\Phi$  because this is likely the most uncertain part of the model.

### 3. Results

#### *a. Arctic Reference Solutions and Sensitivity to $Q$*

Fig. 4 shows results from experiment 1 using parameters roughly appropriate to the Fram Strait and Barents Sea Opening. The parameters (Table 2) are taken from Tsubouchi et al. (2012, 2018). The temperature/salinity diagram in Fig. 4 shows the properties of the various water masses. The OW properties  $T_3, S_3$  range over different values, which correspond to a range of SW salinities  $S_s$ . Notice that the OW and PW properties are moderately realistic compared to the data shown in Fig. 1. The SW salinities are high, however, and the OW properties cluster close to the aW. This fact indicates that the entrainment is high for this solution, and indeed, the mean value is  $\Phi = 0.94$ . Therefore, the shelf circulation is relatively weak and most OW is formed by AW being entrained into the overflowing SW. Hence, the OW temperature  $T_3$  is relatively high and the system balances the heat budget by exporting warm OW. Indeed, experiment 1 has a strong thermal overturning cell compared to the estuarine cell,  $U_3/U_2 \approx 3.4$ , which is moderately realistic (see Fig. 1 and section 1). The ice export flux,  $|U_i|/U_1 \approx 0.040$ , is also moderately realistic.

The blue error bars in Fig. 4 indicate the range of possible solutions for the fixed parameters in experiment 1 (the 0 and 100 percentiles). The bars themselves indicate the solution with entrainment closest to the mean entrainment (other choices are possible). There are two reasons that a range of solutions exists (see supplement section S1). First, for the fluxes in and out of the system as a whole (across section A; left column in Fig. 4), multiple solutions exist for  $\{U_2, U_3, U_i, S_s\}$ , and hence  $\{u_s, T_3, S_3, \Phi\}$ . This multiplicity reflects a tradeoff between shelf salinity  $S_s$  and entrainment  $\Phi$  and is discussed in section 3c. Second, for the fluxes across the shelf break (across section B; right column in Fig. 4), multiple solutions exist for  $u_1$  and  $u_i$  (for every value of  $S_s$ ; the bars show the mean values). This multiplicity reflects a tradeoff between the ocean surface fluxes  $Q_s$  and  $F_s$

on the shelf (it is linear, see (S5)). Physically, this second tradeoff means that the shelf heat budget can be satisfied with relatively large  $Q_s$  (which is positive), large  $u_i$ , large  $\mathcal{F}_s$  (negative), and small  $u_s$ ; or vice versa. The system can lose more or less heat over the shelf relative to the basin, and thereby form more or less sea ice, without disturbing the balance across section A.

Next consider Fig. 5, which shows results from experiment 2. This experiment is the same as experiment 1, except that the total ocean heat loss  $Q$  is one third higher (Table 2). The mass fluxes across section A,  $U_2$  and  $U_3$ , are similar,  $U_3/U_2 \approx 3.8$ . The ice export flux for experiment 2 is also similar,  $|U_i|/U_1 \approx 0.036$ , to experiment 1. Nevertheless, the solution is qualitatively different because it shows strong shelf circulation, cold OW, and weak entrainment (mean  $\Phi = 0.13$ ). In this experiment, to satisfy the heat budget across section A, the OW is cold. That is achieved by the AW flowing onto the shelf, where it is cooled to freezing, and then flowing off the shelf to form OW with little entrainment. The system cannot satisfy the heat budget with a weak shelf circulation, warm OW, and strong entrainment, like in experiment 1. By switching to this other mode of solution (strong shelf circulation), the system accommodates the greater ocean heat loss.

Now consider experiment 3, which extends experiments 1 and 2 to cover a wide range of  $Q$  values (Table 2). Fig. 6 shows the key solution variables as functions of  $Q$ . In each panel, the thick lines show the solution with entrainment closest to the mean entrainment (like the bars in Figs. 4 and 5). The coloured patches show the range of possible solutions (like the error bars in Figs. 4 and 5). Experiments 1 and 2 are shown with solid and dashed lines, respectively. Notice first that the entrainment  $\Phi$  (bottom panel of Fig. 6) reflects the shelf circulation switching on (small  $\Phi$ ) and off (large  $\Phi$ ) according to  $Q$ . Large  $Q$  demands strong shelf circulation to supply a large heat flux from the AW to SW to OW conversion process. Notice next that the range of possible solutions is relatively small for experiments 1 and 2, but between them, at  $Q/(\rho_i L' U_1) \approx 0.09$ , it is large. (Normalizing  $Q$  by  $\rho_i L' U_1$  is natural because it compares the total ocean heat loss to the total

heat that must be extracted to freeze the inflowing AW.) In this case, the relative strengths of the shelf circulation and of the PW/OW mass flux ratio are essentially unconstrained (see section 3d). Finally, notice that the range of possible solutions shrinks to zero for small and large  $Q$  (to the left and right of experiments 1 and 2 in Fig. 6, respectively). At these limits  $U_2$  approaches zero and for  $Q/(\rho_i L' U_1) \lesssim 0.07$  or  $Q/(\rho_i L' U_1) \gtrsim 0.11$ , no negative  $U_2$  solutions are possible. The system no longer makes PW—the hatched regions in Fig. 6—and the estuarine circulation collapses.

*b. Collapse of the Estuarine Overturning Cell: Heat and Salt Crises*

Collapse of the estuarine circulation can occur for two reasons. For small  $Q$ , similar to experiment 1, the shelf circulation is switched off, entrainment is high, and the OW is warm. This state allows maximum export of heat with large OW heat export  $-U_3 T_3$  to compensate for the weak ocean heat loss  $Q$ . Export of PW or sea ice effectively carries away negative heat, or equivalently imports positive heat to the system (because PW is at the freezing temperature and sea ice is deficient in heat; recall the heat budget is constructed relative to  $0^\circ\text{C}$ ). Hence, the only way to increase heat export is to increase  $-U_3 T_3$ . An upper limit to OW temperature  $T_3$  exists, however, which is set by aW temperature  $T_a$  (supplement sections S4–S6). Near this limit (large  $\Phi$ ) the system must compensate for decreased  $Q$  by increased OW export  $-U_3$ . This compensation can only continue as long as the OW mass flux does not exceed the AW mass flux,  $-U_3/U_1 \lesssim 1$ , otherwise the PW flux vanishes. This failure mode (meaning loss of viable solutions) is referred to as *heat crisis* because the system can no longer export enough heat and also maintain the estuarine circulation.

The second reason for collapse of estuarine circulation concerns large  $Q$ , similar to experiment 2. In this case, the shelf circulation is switched on, entrainment is low, and OW is near the freezing temperature. This state restricts the export of heat in the thermal cell to supply the large surface heat loss  $Q \approx Q_s$ . Restricting the export of heat might instead be accomplished by large PW flux

$U_2$  and small OW flux  $U_3$  (OW is also at the freezing temperature). But OW is saltier than PW  $S_3 > S_2$ , so large  $U_3$  and small  $U_2$  is more efficient at exporting salt. In this state ( $U_3 \gg U_2$ ), greater ocean heat loss  $Q$  can be accommodated by more freezing  $u_i$ . More freezing necessarily reduces  $u_s$  and hence  $U_3$ , however, which chokes the export of salt (because sea ice carries very little salt  $S_i \ll S_3$ ). In trying to meet these competing constraints as  $Q$  increases, the system is pushed to vanishing  $U_2$  and collapse of the estuarine circulation. This failure mode is referred to as *salt crisis* because the system can no longer export enough salt and also maintain the estuarine circulation.

### c. Tradeoff between Entrainment and Shelf Circulation

In Figs. 4 and 5 (experiments 1 and 2) we see solutions with similar thermal and estuarine circulations. In both of them, the OW flux dominates the PW flux by a factor of  $U_3/U_2 \approx 3.5$ , which is moderately realistic. The shelf circulation strength  $u_s$  differs by a factor of about 14 between the experiments, however. Understanding how experiments 1 and 2 maintain the same OW/PW ratio despite the large shelf circulation difference illuminates the model.

Figure 7 shows entrainment  $\Phi$  against shelf salinity  $S_s$  for experiments 1 and 2. The solid curve comes from a theoretical argument about the tradeoff between these  $\Phi$  and  $S_s$  (see supplement section S2). For constant  $U_3$ ,

$$\Phi \approx 1 - \frac{\gamma^{3/2}}{\rho_0 \beta \Delta S_s} |U_3|^{1/2}, \quad (12)$$

which says that the shelf salinity anomaly  $\Delta S_s$  and (one minus the) entrainment are inversely proportional to each other. This gives a good fit to the tradeoff between  $\Phi$  and  $S_s$  at fixed  $U_3$  (see Fig. 7). Physically, it reflects the fact that the AW to OW conversion pathway can either occur by strong entrainment and weak shelf circulation (experiment 1) or vice versa (experiment 2). AW can either flow directly into OW through entrainment or it can circulate on the shelf before becoming

OW. As experiments 1 and 2 show, this tradeoff is important for the heat budget, however. Small (large)  $Q$  requires export of warm (cold) OW and therefore a weak (strong) shelf circulation.

*d. Unconstrained OW/PW Fluxes: OW Emergency*

A variation of this idea explains the wide range of possible solutions for intermediate  $Q$ , between experiments 1 and 2 in Fig. 6 (see supplement section S5 for the theory). For  $Q/(\rho_i L' U_1) \approx 0.09$ , the ratio of OW/PW fluxes  $U_3/U_2$  is essentially unconstrained. In this case, solutions exist with strong OW flux and weak PW flux that have weak entrainment, strong shelf circulation and cold OW. These solutions are far from the solid curves in Fig. 6, although still within the coloured patches (to balance mass,  $U_2$  is anti-correlated with  $U_3$  at fixed  $Q$ , as seen from the solid lines). This shelf-dominated mode efficiently supplies AW heat to the shelf and hence to the atmosphere via  $Q_s$ , like experiment 2. But the system also supports solutions with weak OW flux and strong PW flux (unlike experiments 1 and 2). This intermediate- $Q$  mode balances the heat budget by converting AW mainly to PW (which is cold) and suppressing the export of warm OW. It can have either strong or weak entrainment and shelf circulation: the difference between them is unimportant because little AW is converted to OW in the intermediate mode. This type of solution allows vanishing of the OW thermal overturning cell,  $U_3 = 0$ , as the solid curve shows for  $Q/(\rho_i L' U_1) \approx 0.09$ . It is called an *OW emergency*: the thermal cell can disappear, but it does not have to disappear (in contrast, recall that the heat and salt crises require collapse of the estuarine cell). See ahead to section 3g and Fig. 9 for an example of an intermediate- $Q$  solution and OW emergency.

*e. Sensitivity to Other System Parameters*

Experiments 1, 2, and 3 differ only in  $Q$ , the ocean heat loss flux. What about sensitivity to other system parameters? Experiment 4 (Table 2) systematically varies  $\{Q, \mathcal{F}, U_1, T_1, S_1\}$  in 1769472



different combinations ( $\phi = 0.33$  is held constant: see section 3f and supplement section S4). Experiment 4 spans the space of parameters for the Fram Strait and Barents Sea Opening, arising from uncertainty or secular variability. Fig. 8 shows the results for the export volume fluxes. The figure shows histograms of the volume fluxes plotted against

$$\mathcal{N}^* \equiv (1 - S_i/S_1)Q + L'\mathcal{F} + c_p\rho_1(S_i/S_1 - 1)T_1U_1, \quad (13)$$

$$\approx Q + L\mathcal{F} - c_p\rho_0U_1T_1, \quad (14)$$

$$\approx \rho_i L' (U_1 + U_2 + U_3). \quad (15)$$

The origin of  $\mathcal{N}^*$  is explained in supplement section S3 and its physical interpretation is discussed below. This compound forcing parameter is a function of (mainly)  $Q, \mathcal{F}$ , and  $U_1T_1$ . It collapses the five dimensional  $\{Q, \mathcal{F}, U_1, T_1, S_1\}$  parameter space onto a line. Distance along this line,  $\mathcal{N}^*$ , is proportional to  $Q$ , but it also depends on the other parameters. In this way,  $\mathcal{N}^*$  in experiment 4 and Fig. 8 generalizes  $Q$  in experiment 3 and Fig. 6. The histograms are constructed from the mean entrainment solutions, like the bars in Fig. 4, and the results from experiment 3 are shown with white curves on Fig. 8 for reference. Most of the variation in  $U_2$  among the solutions is controlled by  $\mathcal{N}^*$ , indicating that this parameter dominates these variations. Equivalently, for a fixed  $\mathcal{N}^*$  value, the distribution of  $U_2$  values is relatively tight, especially for  $U_2 \rightarrow 0$  approaching the heat and salt crises. For example, the range of  $U_2$  values for fixed  $\mathcal{N}^*$  is typically smaller than the range of  $U_2$  values about the mean entrainment solution seen in Fig. 4. Similar remarks apply to the distribution of  $U_3$ .

Physically,  $\mathcal{N}^*$  generalizes the ocean heat loss flux parameter  $Q$ . In particular,  $\mathcal{N}^*/(\rho_i L' U_1)$  is the fractional anomaly in the volume budget  $U_1 + U_2 + U_3 \approx \mathcal{N}^*/(\rho_i L)$ , meaning that  $\mathcal{N}^*$  measures the (small) difference between the AW transport and the OW and PW transports. This difference is approximately the meteoric freshwater flux  $\mathcal{F}/\rho_i$  plus the sea ice export  $U_i$ . Supplement section

S3 shows theoretical support (see (S12)), but the main evidence is that the results of experiment 4 in Fig. 8 plotted against  $N^*$  resemble those from experiment 3 in Fig. 6 plotted against  $Q$ . In particular, the types of solution and failure mode are the same in experiments 3 and 4.

*f. Sensitivity to PW salinity  $S_2$  and Mixing Fraction  $\phi$ : Entrainment Emergency*

Recall, that the AW to PW conversion model (section 2) sets an upper limit for the PW salinity. In all experiments shown so far, the PW salinity  $S_2$  equals this limit from (3). This assumption is now relaxed, as is the related assumption that aW has a fixed mixing fraction  $\phi$ .

Experiment 5 varies  $S_2$  with all other parameters fixed as for experiment 1 (Table 2, Fig. S2). There exists a range of possible solutions at moderate entrainment values. As  $S_2$  decreases, the estuarine cell strength  $U_2$  weakens as for the salt and heat crises. For a certain  $S_2 \approx 33.5$  g/kg,  $U_2$  vanishes and the estuarine cell disappears. This crisis differs from the salt and heat crises, however, because entrainment  $\Phi \approx 0.63$  (not zero or one). It is called an *entrainment emergency*. Approaching the entrainment emergency, the aW salinity  $S_a$  decreases because the PW salinity  $S_2$  is decreasing. The OW salinity  $S_3$  therefore also decreases. The OW salinity can only decrease until the OW density  $\rho_3$  equals the AW density  $\rho_1$ , however, otherwise the stable stratification of AW above OW fails. Therefore, a crisis occurs beyond which entrainment of aW into overflowing shelf water to form OW is no longer possible. The aW becomes too light (fresh) for solutions to the entrainment model to exist. This entrainment emergency also occurs for large  $\phi$  values that make the aW too fresh, for the same reason (see supplement Fig. S3d).

The model specifies the mixing fraction  $\phi$ . An objection to this choice is that  $\phi$  might more realistically depend on the PW salinity. Entrainment of PW into the descending SW plume might be less likely if PW is less dense (fresher) than AW, for example. That argues for  $\phi$  to depend on  $\rho_1 - \rho_2$ . This possibility is not pursued here because the function  $\phi(\rho_1 - \rho_2)$  is unknown.

Instead, consider the choice  $\phi = 0$  so that aW and AW properties are the same: Because the aW properties are independent of SW salinity for  $\phi = 0$ , the entrainment emergency disappears. The route for meteoric freshwater and sea ice melt to enter the thermal overturning is also eliminated. However, there is no qualitative effect on experiments 1–3 (not shown). There is negligible effect on shelf-dominated solutions (like experiment 2) because entrainment is unimportant for them. For entrainment-dominated solutions (experiment 1), the OW temperature and salinity increase somewhat (which is less realistic) with marginal changes in transport fluxes.

*g. Antarctic Reference Solution and Choice of  $\gamma$*

Figure 9 shows a canonical Antarctic solution (experiment 6). The parameters (Table 2) are taken from Abernathey et al. (2016); Price and O’Neil Baringer (1994) and Volkov et al. (2010). They represent (crudely) the meridional overturning circulation at all longitudes, consistent with the paradigm of zonal-average overturning in the Southern Ocean (Talley 2013; Abernathey et al. 2016; Pellichero et al. 2018). The solution in Fig. 9 has a wide range of OW water properties, entrainment values, and shelf salinities. The canonical solution has  $U_2 \approx -16$  Sv,  $U_3 \approx -10$  Sv, and  $u_i \approx -0.27$  Sv, which are moderately realistic values (Abernathey et al. 2016; Pellichero et al. 2018). The PW flux nearly always exceeds the OW flux and the system is close to OW emergency. In this sense, the system is more loosely constrained than experiments 1 and 2 and further from heat and salt crises. It is close to switching between strong and weak shelf circulation (Fig. 6).

The values for the parameters in the Antarctic reference case are uncertain. For example, it is unclear what AW temperature to pick. The value used in experiment 6 is  $0.5^\circ\text{C}$ , which reflects the temperature adjacent to the Antarctic shelf in the Weddell Sea. The temperature at the Polar Front is warmer, by about a degree Celsius (Smedsrud 2005). The present model cannot handle latitudinal variations in AW temperature, however. Increasing  $T_1$  from  $0.5$  to  $1.5^\circ\text{C}$  moves the

Antarctic solution towards an entrainment-dominated solution like experiment 1. The transports are about the same, but with slightly stronger (weaker) OW (PW). The possibility of OW emergency is less, entrainment is higher, and the OW is warmer.

The Antarctic reference solution reveals an important issue, namely, the choice of entrainment parameter  $\gamma$  from (9). Recall from section 2a that  $\gamma$  sets the sensitivity of entrainment to changes in overflowing SW flux and density difference. For the Arctic experiments 1–5,  $\gamma = 2.2 \times 10^{-3} \text{ kg}^{2/3} \text{ s}^{1/3} \text{ m}^{-3}$ , which derives from Price and O’Neil Baringer (1994) (their Table 1). The main  $\gamma$  uncertainty is in  $W_s + 2K_{\text{geo}}x$ , where  $W_s$  is the overflow plume width,  $K_{\text{geo}}$  is the geostrophic Ekman number, and  $x$  is downstream distance. This sum is dominated by the plume width  $W_s$  for the cases shown here, so focus on  $W_s$ . How should  $W_s$  vary with the inflow flux  $U_1$ , which sets the circulation scale for the problem? The simplest choice, adopted here, is to make  $W_s$  proportional to  $U_1$ . Physically, that means the shelf system can accommodate arbitrarily broad overflow plumes (technically, it means the problem is linear in  $U_1$ ). This choice cannot be true for all possible  $U_1$  fluxes because the shelf break length is limited. But for experiments 1 and 6,  $W_s = 100$  and  $550\text{km}$ , respectively, which are short compared to the lengths of the Siberian and Antarctic shelves so the choice appears plausible. In any case,  $\gamma$  has little effect on salt crises because entrainment vanishes for them, or on the possibility of OW emergencies.

#### 4. Discussion

The model constructed here combines well-established principles. The main principles are: (i) conservation of mass, salt, and heat, (ii) the Price and O’Neil Baringer (1994) overflow plume model, which is frictional-geostrophic and mixes at hydraulic jumps, and (iii) linear mixing. The ancillary principles are: (iv) static stability of PW, AW, OW, and SW, and (v) constraints on the sense of circulation, for example to ensure the system exports sea ice and does not import it.

Conservation laws on their own are not enough to close the system (Eldevik and Nilsen 2013). The Price and O'Neil Baringer (1994) overflow plume model requires as input parameters the aW properties and SW properties and flux, so it is also not closed. Conservation laws and the plume model together give a closed system. The parametrization of mixing at hydraulic jumps in the plume model is nonlinear, which means that either no solutions are possible, or an infinite number. The ancillary principles exclude physically unrealistic solutions. The model solutions consist of fluxes of PW, OW, SW, and sea ice, and OW properties (plus related variables). The model principles are plausible, but many variants are possible for future study.

Fig. 10 shows a schematic of the main solution modes for this model. The quantitative details of the experiments depend on specific parameter choices, but the qualitative solution modes do not. These modes are organized by PW collapse (loss of the estuarine cell) in heat and salt crises; by unconstrained tradeoff between PW and OW in OW emergency (possible loss of the overturning cell); and by entrainment emergency (loss of the estuarine cell). The sign of the solution sensitivity to forcing parameters depends on the solution location with respect to the crises and emergencies. For example, the estuarine PW cell strengthens as  $Q$  increases if entrainment dominates and OW is warm (like experiment 1 in Fig. 6). But the estuarine cell weakens as  $Q$  increases if shelf circulation dominates and OW is cold (like experiment 2). The sensitivity of the sea ice export flux to  $Q$  also changes sign like this (Figs. 6 and 8). OW thermohaline properties are insensitive to forcing parameters, except when the system switches between strong and weak shelf circulation near the OW emergency. Then, the OW temperature (but not salinity) is very sensitive to forcing changes, which leads to a bimodal distribution of OW temperature (Fig. 6). The OW properties are buffered to changes in shelf salinity in this way. The corollary is that the shelf salinity is relatively unconstrained by the OW properties reflecting the tradeoff between entrainment and shelf circulation (Fig. 7).

The transition between modes is mainly controlled by the compound forcing parameter  $\mathcal{N}^*$  (section 3e, eqs. (13)–(15)), which generalizes the effect of the ocean heat loss rate  $Q$ . The  $\mathcal{N}^*$  parameter estimates the departure from the closed volume budget between AW, OW, and PW. It shows that heat and freshwater flux changes are interchangeable: greater ocean heat loss compensates greater ocean freshwater gain, and vice versa. If the changes are due to ice melt (or freezing) then there is no net change in  $\mathcal{N}^*$ . That means that greater (or less) ocean heat loss to Antarctic land ice, for example, makes (almost) no change to the solution. Similarly, only the difference between  $Q$  and AW heat flux matters, not the individual magnitudes, and the AW salt flux is unimportant. These results emerge from the mass, salt, and heat budgets so they are robust.

The main approximation in this model is the Price and O’Neil Baringer (1994) entrainment parametrization. In particular, uncertainty surrounds the functional form (9), the entrainment sensitivity parameter  $\gamma$ , and the aW properties (from PW salinity  $S_2$  and mixing fraction  $\phi$ ). Still, the entrainment model is based on firm physical principles. Price and O’Neil Baringer (1994) couple entrainment to the dynamics of the overflow plume, which is the key ingredient in the present model. They are guided by the laboratory experiments of Ellison and Turner (1959) and Turner (1986). These studies suggest that mixing during entrainment events is so efficient that the Froude number cannot exceed one. The assumption of geostrophic flow, and thus a geostrophic Froude number in (8), implies the two-thirds exponent in the Froude number scaling (7) (J. Price, pers. comm.). A different exponent would change the details of the switch between strong and weak shelf circulation magnitudes, but not the existence of the switching. Other studies on overflow entrainment point to the importance of entrainment for subcritical flows (Froude number  $<1$ , Cenedese and Adduce 2010), especially over rough bottoms (Ottolenghi et al. 2017). Boosting of entrainment by tidal currents is also thought to be important in some situations, such as for AABW in the Ross Sea (Padman et al. 2009). These additional effects are worth exploring, but appear

unlikely to make a qualitative difference because few solutions have subcritical flow and vanishing entrainment (Figs. 6, 8). Likely more important is to revisit the assumption of efficient entrainment controlled by the Froude number. For example, Akimova et al. (2011) constructed a model for the Storfjorden plume, which is one of the better-documented Arctic shelf overflows. They found that the entrainment assumptions of Ellison and Turner (1959) and Price and O'Neil Baringer (1994) put too much entrainment at the shelf break. Better results were obtained by relating entrainment to the plume volume transport, which puts most of the entrainment in the deeper layers.

Consider now the maximum SW salinity  $S_s^{\max}$  (see supplement sections S1 and S4). This parameter is unavoidable in the numerical method because the entrainment parametrization (9) involves a power law of the aW/SW density (hence salinity) difference. Therefore, no characteristic maximum shelf salinity exists. The upper limit on SW salinity is controlled in reality by other processes. Most important is exchange across the shelf break jet unrelated to dense overflows, like baroclinic instability (Lambert et al. 2018; Stewart et al. 2018). This exchange augments dense overflows in exporting salt from the shelf (and importing heat on to the shelf). The relative importance of these shelf break exchange mechanisms and their interaction are unclear and worth exploring. The key question is how they control (in order of priority) the OW temperature, OW salinity, and PW salinity because once these variables are known, the budget equations (S1) specify the transports. Despite the uncertainty in what sets  $S_s^{\max}$ , the results from experiment 5 with a wide range of forcing parameters show that the value chosen here is unimportant: The mean, median, and modal excess SW salinities over AW salinities are just 0.67, 0.04, and -0.06 g/kg, respectively. These are reasonable values compared to the observations mentioned in section 1.

Several other potentially important processes are excluded. Among them are pressure-dependent effects in seawater density, such as thermobaricity (Killworth 1977; Stewart and Haine 2016). Correcting for thermobaricity would increase the SW density relative to the aW density (because

SW is colder and more compressible). That effect enhances entrainment although it is probably small as the entrainment does not occur at great depths. Cabbeling is also ignored, which is important for mixing at strong thermohaline fronts (Stewart et al. 2017) and potentially for upwelling of CDW in the Southern Ocean (Evans et al. 2018). The linear mixing formulae (like (10)–(11)) include cabbeling, but the impact on stratifying the water column is beyond the scope of this model. Interaction with ice sheets is also potentially important, especially in the Antarctic where glacial melt is significant (Jenkins et al. 2016; Abernathy et al. 2016; Dinniman et al. 2016). This source of freshwater depends on the ocean heat flux to the ice sheet, but the freshwater flux is specified here, regardless of the shelf circulation. Indeed, both the freshwater flux and the ocean heat loss flux  $Q$  are specified independently of the system state. They are also allowed to freely vary between shelf and basin, with only their sums constrained (supplement section S1). These assumptions are unrealistic because  $Q$ , for instance, depends on sea ice cover. Only steady solutions are shown, but in the real system time-dependent solutions may be important too, and they are intrinsically interesting. For time-dependence the model equations must be expanded to include water mass reservoir volumes, which will control the characteristic time scales for transient adjustment. One possibility is to couple the shelf and basin so they can exchange heat and salt anomalies. This coupling may resolve the degeneracy near the OW emergency into periodic solutions.

## 5. Conclusions

This paper reports a conceptual model that specifies the strengths and thermohaline properties of polar estuarine and thermal overturning cells. The model satisfies mass, salt, and heat budgets plus physical parametrizations for PW and OW formation. We explore the model characteristics and apply it to the Arctic and Antarctic termini of the global ocean overturning circulation. At best, the conceptual model is a caricature of a piece of the real system. It is most useful where



it suggests characteristics of the estuarine and thermal overturning cells that are robust in more realistic models. Then it guides further research. The salient model characteristics are:

- The system is controlled by five flux parameters, namely the inflowing mass, heat, and freshwater fluxes, and the air/sea/ice heat and freshwater fluxes. However, the state is dominated by a single forcing parameter (eq. (13)) that is a linear combination of ocean heat loss flux, inflowing heat flux and ocean freshwater flux. This parameter measures the departure from a balanced volume budget between the estuarine and thermal overturning cells.
- A one-parameter infinity of solutions typically exists but the range of possible solutions can be tight. The solutions have different circulations onto and off the continental shelf, which links to overflow entrainment. This tradeoff permits switching between two states: the states exhibit strong (weak) shelf circulation, weak (strong) overflow entrainment, and large (small) heat flux from the ocean to the atmosphere. Switching allows the system to accommodate a wide range of inflow and air/sea/ice exchange fluxes and gives a bi-modal distribution of OW temperature with a narrow range of OW salinity.
- Solutions exist for limited flux parameters. Solutions disappear if the heat (salt) budget fails to balance because the system cannot export enough heat (salt). These heat (salt) crises collapse the estuarine cell. The thermal overturning cell can collapse in a so-called OW emergency, but it does not have to.
- For the Arctic, specifically the transfer across the Fram Strait and Barents Sea Opening, the real system appears vulnerable to heat crisis. The estuarine cell vanishes for increased meteoric freshwater flux to the ocean, or increased AW heat flux, or decreased ocean heat loss flux. The first two factors are anticipated under global warming (Rawlins et al. 2010; Vavrus

et al. 2012; Collins et al. 2013), pushing the Arctic closer to heat crisis and collapse of the estuarine cell. This may relate to Arctic Ocean “Atlantification” (Polyakov et al. 2017).

- For the Antarctic, the real system appears close to OW emergency with weak constraints on the strengths of the estuarine and thermal cells, although most solutions show a stronger estuarine cell. This result suggests that the Antarctic system is more susceptible to unforced variations than the Arctic. The sensitivity of the Antarctic solutions to changes in flux parameters is unclear because the system appears close to switching between strong and weak shelf circulation modes. Loss of parts of the estuarine cell may relate to loss of sea ice and PW in Weddell Sea polynyas (Comiso and Gordon 1987; Gordon 2014). Such offshore polynyas are linked to climate variations that are projected to strengthen with anthropogenic climate change (Campbell et al. 2019). Loss of the thermal cell may relate to loss of AABW formation due to increased land ice melt in future climate projections (Lago and England 2019). Warming CDW (Smedsrud 2005) pushes the Antarctic system towards the entrainment-dominated solution with warm OW and weak shelf circulation (Fig. 10a).

The most important lessons from this conceptual polar overturning model are probably these: The model Arctic regime is being driven towards heat crisis and collapse of the estuarine overturning cell by flux changes associated with anthropogenic climate change. Approaching the heat crisis, entrainment and shelf salinity are high, shelf circulation is weak, and variability in OW flux and temperature is small. Sea ice does not disappear prior to the heat crisis. The model Antarctic regime shows large intrinsic variability between OW and PW fluxes and between strong and weak shelf circulations. The magnitude and sign of the sensitivity to changes in ocean heat loss, freshwater gain, and CDW heat flux are uncertain. But sensitivity is weak to changes due to oceanic melting of glacial ice.

Future work should vary the model principles, and there are many ways to do so. Most important will be to modify the assumptions on sea ice, for example, to allow sea ice to control the ocean heat loss rate, to allow freezing in the basin, and to add a seasonal cycle. Allowing for PW to gain density by brine rejection from freezing admits the possibility of a new circulation mode: namely, deep convection through the AW.

*Data availability statement.* The MATLAB software to compute solutions to the conceptual model in this paper is available at [github.com/hainegroup/Polar-overturning-circulation-model](https://github.com/hainegroup/Polar-overturning-circulation-model). An interactive app. and the scripts to produce the figures are available.

*Acknowledgments.* This work was supported by grant 19-PO19-0025 from the National Aeronautics and Space Administration. Discussions with Ali Siddiqui, Miguel Jimenez-Urias, and Renske Gelderloos helped clarify the work and Bert Rudels inspired it.

## References

- Aagaard, K., L. K. Coachman, and E. Carmack, 1981: On the halocline of the Arctic Ocean. *Deep Sea Res., Part A*, **28 (6)**, 529–545, doi:10.1016/0198-0149(81)90115-1.
- Aagaard, K., J. H. Swift, and E. C. Carmack, 1985: Thermohaline circulation in the Arctic Mediterranean Seas. *J. Geophys. Res.*, **90 (C3)**, 4833, doi:10.1029/jc090ic03p04833.
- Abernathey, R. P., I. Cerovecki, P. R. Holland, E. Newsom, M. Mazloff, and L. D. Talley, 2016: Water-mass transformation by sea ice in the upper branch of the Southern Ocean overturning. *Nature Geoscience*, **9 (8)**, 596–601, doi:10.1038/ngeo2749.

- Akimova, A., U. Schauer, S. Danilov, and I. Núñez-Riboni, 2011: The role of the deep mixing in the Storfjorden shelf water plume. *Deep Sea Res., Part I*, **58** (4), 403–414, doi:10.1016/j.dsr.2011.02.001.
- Boyer, T. P., and Coauthors, 2018: World ocean database 2018. Tech. rep., NOAA Atlas NESDIS 87. [https://data.nodc.noaa.gov/woa/WOD/DOC/wod\\_intro.pdf](https://data.nodc.noaa.gov/woa/WOD/DOC/wod_intro.pdf).
- Campbell, E. C., E. A. Wilson, G. W. K. Moore, S. C. Riser, C. E. Brayton, M. R. Mazloff, and L. D. Talley, 2019: Antarctic offshore polynyas linked to Southern Hemisphere climate anomalies. *Nature*, **570** (7761), 319–325, doi:10.1038/s41586-019-1294-0.
- Cenedese, C., and C. Adduce, 2010: A new parameterization for entrainment in overflows. *J. Phys. Oceanogr.*, **40** (8), 1835–1850, doi:10.1175/2010jpo4374.1.
- Cerovečki, I., L. D. Talley, M. R. Mazloff, and G. Maze, 2013: Subantarctic Mode Water formation, destruction, and export in the eddy-permitting Southern Ocean State Estimate. *J. Phys. Oceanogr.*, **43** (7), 1485–1511, doi:10.1175/jpo-d-12-0121.1.
- Collins, M., and Coauthors, 2013: Long-term climate change: Projections, commitments and irreversibility. *Climate Change 2013: The Physical Science Basis. Contribution of Working Group I to the Fifth Assessment Report of the Intergovernmental Panel on Climate Change*, T. F. Stocker, D. Qin, G.-K. Plattner, M. Tignor, S. K. Allen, J. Boschung, A. Nauels, Y. Xia, V. Bex, and P. M. Midgley, Eds., Cambridge University Press, Cambridge, United Kingdom and New York, NY, USA.
- Comiso, J. C., and A. L. Gordon, 1987: Recurring polynyas over the Cosmonaut Sea and the Maud Rise. *J. Geophys. Res.*, **92** (C3), 2819, doi:10.1029/jc092ic03p02819.

- Dinniman, M., X. Asay-Davis, B. Galton-Fenzi, P. Holland, A. Jenkins, and R. Timmermann, 2016: Modeling ice shelf/ocean interaction in Antarctica: A review. *Oceanography*, **29** (4), 144–153, doi:10.5670/oceanog.2016.106.
- Eldevik, T., and J. E. Ø. Nilsen, 2013: The Arctic–Atlantic thermohaline circulation. *J. Climate*, **26** (21), 8698–8705, doi:10.1175/jcli-d-13-00305.1.
- Ellison, T. H., and J. S. Turner, 1959: Turbulent entrainment in stratified flows. *J. Fluid Mech.*, **6** (03), 423, doi:10.1017/s0022112059000738.
- Evans, D. G., J. D. Zika, A. C. Naveira Garabato, and A. J. G. Nurser, 2018: The cold transit of Southern Ocean upwelling. *Geophys. Res. Lett.*, **45** (24), 13,386–13,395, doi:10.1029/2018gl079986.
- Foster, T. D., and E. C. Carmack, 1976: Frontal zone mixing and Antarctic bottom water formation in the southern Weddell Sea. *Deep Sea Res.*, **23**, 301–317.
- Gao, L., S. R. Rintoul, and W. Yu, 2017: Recent wind-driven change in Subantarctic Mode Water and its impact on ocean heat storage. *Nature Climate Change*, **8** (1), 58–63, doi:10.1038/s41558-017-0022-8.
- Gill, A. E., 1973: Circulation and bottom water production in the Weddell Sea. *Deep Sea Res.*, **20**, 111–140, doi:10.1016/0011-7471(73)90048-x.
- Gordon, A. L., 2014: Southern Ocean polynya. *Nature Climate Change*, **4** (4), 249–250, doi:10.1038/nclimate2179.
- Haine, T. W. N., and Coauthors, 2015: Arctic freshwater export: Status, mechanisms, and prospects. *Glob. Planet. Change*, **125**, 13–35, doi:10.1016/j.gloplacha.2014.11.013.

- Hansen, B., and S. Østerhus, 2000: North Atlantic-Nordic Seas exchange. *Prog. Oceanogr.*, **45**, 109–208, doi:10.1016/s0079-6611(99)00052-x.
- Hansen, B., S. Østerhus, W. R. Turrell, S. Jónsson, H. Valdimarsson, H. Hátún, and S. M. Olsen, 2008: The inflow of Atlantic water, heat, and salt to the Nordic Seas across the Greenland-Scotland ridge. *Arctic-Subarctic Ocean Fluxes: Defining the role of the Northern Seas in Climate*, R. R. Dickson, J. Meincke, and P. Rhines, Eds., Springer-Verlag, 15–43, doi:10.1007/978-1-4020-6774-7\_2.
- Haumann, F. A., N. Gruber, M. Münnich, I. Frenger, and S. Kern, 2016: Sea-ice transport driving Southern Ocean salinity and its recent trends. *Nature*, **537 (7618)**, 89–92, doi:10.1038/nature19101.
- Jacobs, S. S., 2004: Bottom water production and its links with the thermohaline circulation. *Antarctic Science*, **16 (4)**, 427–437, doi:10.1017/s095410200400224x.
- Jenkins, A., P. Dutrieux, S. Jacobs, E. Steig, H. Gudmundsson, J. Smith, and K. Heywood, 2016: Decadal ocean forcing and Antarctic ice sheet response: Lessons from the Amundsen Sea. *Oceanography*, **29 (4)**, 106–117, doi:10.5670/oceanog.2016.103.
- Killworth, P. D., 1977: Mixing on the Weddell Sea continental slope. *Deep Sea Res.*, **24**, 427–448.
- Klinger, B. A., and T. W. N. Haine, 2019: *Ocean Circulation in Three Dimensions*. 1st ed., Cambridge University Press, Cambridge, United Kingdom and New York, NY, USA, URL <http://www.cambridge.org/9780521768436>.
- Lago, V., and M. H. England, 2019: Projected slowdown of Antarctic bottom water formation in response to amplified meltwater contributions. *J. Climate*, **32 (19)**, 6319–6335, doi:10.1175/jcli-d-18-0622.1.

- Lambert, E., T. Eldevik, and M. A. Spall, 2018: On the dynamics and water mass transformation of a boundary current connecting alpha and beta oceans. *J. Phys. Oceanogr.*, **48** (10), 2457–2475, doi:10.1175/jpo-d-17-0186.1.
- Marshall, J., and K. Speer, 2012: Closure of the meridional overturning circulation through Southern Ocean upwelling. *Nature Geoscience*, **5**, 171–180, doi:10.1038/ngeo1391.
- Maus, S., 2003: Interannual variability of dense shelf water salinities in the north-western Barents Sea. *Polar Research*, **22** (1), 59–66, doi:10.3402/polar.v22i1.6444.
- McCartney, M. S., 1977: Subantarctic Mode Water. *A Voyage of Discovery: George Deacon 70th Anniversary Volume, Supplement to Deep-Sea Research*, Pergamon.
- Muench, R., L. Padman, A. Gordon, and A. Orsi, 2009: A dense water outflow from the Ross Sea, Antarctica: Mixing and the contribution of tides. *J. Mar. Res.*, **77** (4), 369–387, doi:10.1016/j.jmarsys.2008.11.003.
- Naveira Garabato, A. C., E. L. McDonagh, D. P. Stevens, K. J. Heywood, and R. J. Sanders, 2002: On the export of Antarctic Bottom Water from the Weddell Sea. *Deep Sea Res., Part II*, **49** (21), 4715–4742, doi:10.1016/s0967-0645(02)00156-x.
- Nicholls, K. W., S. Østerhus, K. Makinson, T. Gammelsrød, and E. Fahrbach, 2009: Ice-ocean processes over the continental shelf of the southern Weddell Sea, Antarctica: A review. *Rev. Geophys.*, **47** (3), doi:10.1029/2007RG000250.
- Orsi, A. H., G. C. Johnson, and J. L. Bullister, 1999: Circulation, mixing, and production of Antarctic bottom water. *Prog. Oceanogr.*, **43**, 55–109, doi:10.1016/s0079-6611(99)00004-x.

- Østerhus, S., W. R. Turrell, S. Jónsson, and B. Hansen, 2005: Measured volume, heat, and salt fluxes from the Atlantic to the Arctic Mediterranean. *Geophys. Res. Lett.*, **32**, doi:10.1029/2004GL022188.
- Ottolenghi, L., C. Cenedese, and C. Adduce, 2017: Entrainment in a dense current flowing down a rough sloping bottom in a rotating fluid. *J. Phys. Oceanogr.*, **47** (3), 485–498, doi:10.1175/jpo-d-16-0175.1.
- Padman, L., S. L. Howard, A. H. Orsi, and R. D. Muench, 2009: Tides of the northwestern Ross Sea and their impact on dense outflows of Antarctic Bottom Water. *Deep Sea Res., Part II*, **56** (13-14), 818–834, doi:10.1016/j.dsr2.2008.10.026.
- Pellichero, V., J.-B. Sallée, C. C. Chapman, and S. M. Downes, 2018: The southern ocean meridional overturning in the sea-ice sector is driven by freshwater fluxes. *Nature Communications*, **9** (1), doi:10.1038/s41467-018-04101-2.
- Polyakov, I. V., and Coauthors, 2017: Greater role for Atlantic inflows on sea-ice loss in the Eurasian Basin of the Arctic Ocean. *Science*, **356** (6335), 285–291, doi:10.1126/science.aai8204.
- Price, J. F., and M. O’Neil Baringer, 1994: Outflows and deep water production by marginal seas. *Prog. Oceanogr.*, **33**, 161–200, doi:10.1016/0079-6611(94)90027-2.
- Quadfasel, D., B. Rudels, and K. Kurz, 1988: Outflow of dense water from a Svalbard fjord into the Fram Strait. *Deep Sea Res., Part A*, **35** (7), 1143–1150, doi:10.1016/0198-0149(88)90006-4.
- Rawlins, M. A., and Coauthors, 2010: Analysis of the Arctic system for freshwater cycle intensification: Observations and expectations. *J. Climate*, **21**, 5715–5737, doi:10.1175/2010JCLI3421.1.
- Rudels, B., 2010: Constraints on exchanges in the Arctic Mediterranean—do they exist and can they be of use? *Tellus*, **62A**, 109–122, doi:10.1111/j.1600-0870.2009.00425.x.



- Rudels, B., 2012: Arctic Ocean circulation and variability - advection and external forcing encounter constraints and local processes. *Ocean Sci.*, **8**, 261–286, doi:10.5194/os-8-261-2012.
- Rudels, B., 2016: Arctic Ocean stability: The effects of local cooling, oceanic heat transport, freshwater input, and sea ice melt with special emphasis on the Nansen basin. *J. Geophys. Res.*, **121**, doi:10.1002/2015JC011045.
- Rudels, B., E. Fahrbach, J. Meincke, G. Budéus, and P. Eriksson, 2002: The East Greenland Current and its contribution to the Denmark Strait overflow. *ICES J. Mar. Sci.*, **59**, 1133–1154, doi:10.1006/jmsc.2002.1284.
- Rudels, B., and D. Quadfasel, 1991: Convection and deep water formation in the Arctic Ocean-Greenland Sea system. *J. Mar. Sys.*, **2 (3-4)**, 435–450, doi:10.1016/0924-7963(91)90045-v.
- Smedsrud, L. H., 2005: Warming of the deep water in the Weddell Sea along the Greenwich meridian: 1977–2001. *Deep Sea Res., Part I*, **52 (2)**, 241–258, doi:10.1016/j.dsr.2004.10.004.
- Stewart, A. L., A. Klocker, and D. Menemenlis, 2018: Circum-Antarctic shoreward heat transport derived from an eddy- and tide-resolving simulation. *Geophys. Res. Lett.*, **45 (2)**, 834–845, doi:10.1002/2017gl075677.
- Stewart, K. D., and T. W. N. Haine, 2016: Thermobaricity in the transition zones between alpha and beta oceans. *J. Phys. Oceanogr.*, **46 (6)**, 1805–1821, doi:10.1175/jpo-d-16-0017.1.
- Stewart, K. D., T. W. N. Haine, A. M. Hogg, and F. Roquet, 2017: On cabbelling and thermobaricity in the surface mixed layer. *J. Phys. Oceanogr.*, **47**, 1775–1787, doi:10.1175/jpo-d-17-0025.1.
- Talley, L., 2013: Closure of the global overturning circulation through the Indian, Pacific, and Southern Oceans: Schematics and transports. *Oceanography*, **26 (1)**, 80–97, doi:10.5670/oceanog.2013.07.

- Tamura, T., and K. I. Ohshima, 2011: Mapping of sea ice production in the Arctic coastal polynyas. *J. Geophys. Res.*, **116** (C7), doi:10.1029/2010jc006586.
- Tsubouchi, T., and Coauthors, 2012: The Arctic Ocean in summer: A quasi-synoptic inverse estimate of boundary fluxes and water mass transformation. *J. Geophys. Res.*, **117** (C1), C01 024, doi:10.1029/2011JC007174.
- Tsubouchi, T., and Coauthors, 2018: The Arctic Ocean seasonal cycles of heat and freshwater fluxes: observation-based inverse estimates. *J. Phys. Oceanogr.*, **48** (9), 2029–2055, doi:10.1175/jpo-d-17-0239.1.
- Turner, J. S., 1986: Turbulent entrainment: the development of the entrainment assumption, and its application to geophysical flows. *J. Fluid Mech.*, **173**, 431–471, doi:10.1017/s0022112086001222.
- Vavrus, S. J., M. M. Holland, A. Jahn, D. Bailey, and B. A. Blazey, 2012: Twenty-first-century Arctic climate change in CCSM4. *J. Climate*, **25**, 2696–2710, doi:10.1175/JCLI-D-11-00220.1.
- Volkov, D. L., L.-L. Fu, and T. Lee, 2010: Mechanisms of the meridional heat transport in the Southern Ocean. *Ocean. Dyn.*, **60** (4), 791–801, doi:10.1007/s10236-010-0288-0.

## LIST OF TABLES

- Table 1.** Notation. AW = Atlantic Water (subscript 1), PW = Polar Water (subscript 2), OW = Overflow Water (subscript 3), aW = ambient Water (subscript a). See also Fig. 2. . . . . 35
- Table 2.** Experiments. The mixing fraction  $\phi = 0.33$ ; see section 3f for a discussion. For all experiments  $\delta\Phi = 0.01$  (see supplement section S1),  $T_i = -10^\circ\text{C}$ ,  $S_i = 4 \text{ g/kg}$ . . . . . 37

TABLE 1. Notation. AW = Atlantic Water (subscript 1), PW = Polar Water (subscript 2), OW = Overflow Water (subscript 3), aW = ambient Water (subscript a). See also Fig. 2.

Symbol	Unit	Meaning
Parameters		
$U_1, T_1, S_1$	Sv, °C, g/kg	AW volume flux, temperature, salinity at gateway
$Q = Q_b + Q_s$	W	Ocean heat flux (total = basin + shelf)
$\mathcal{F} = \mathcal{F}_b + \mathcal{F}_s$	kg s <sup>-1</sup>	Ocean freshwater mass flux (total = basin + shelf)
$\phi$	(no unit)	Mass fraction of PW to AW entrained into OW
$\mathcal{N}^*$	W	Compound forcing parameter from (13)
Variables		
$U_2, U_3, U_i$	Sv	PW, OW, sea ice volume flux at gateway
$u_1, u_i$	Sv	AW, sea ice volume flux at shelf break
$S_s$	g/kg	SW salinity
Intermediate variables		
$S_2$	g/kg	PW salinity
$T_3, S_3$	°C, g/kg	OW temperature, salinity
$T_a, S_a$	°C, g/kg	aW temperature, salinity
$u_s$	Sv	SW volume flux at shelf break
$\rho_1, \rho_2, \rho_3, \rho_a$	kg m <sup>-3</sup>	AW, PW, OW, aW density
$\Phi$	(no unit)	Entrainment mass fraction

Continued on next page.

Table 1 continued.

Symbol	Unit	Meaning
Constants		
$T_i, S_i$	$^{\circ}\text{C}, \text{g/kg}$	Sea ice temperature, salinity
$T_2 = T_s = T_f$	$^{\circ}\text{C}$	PW, SW, freezing temperature
$\rho_i, \rho_0$	$\text{kgm}^{-3}$	Sea ice, characteristic seawater density
$c_p, c_i$	$\text{Jkg}^{-1}\text{K}^{-1}$	Seawater, sea ice specific heat capacity
$L$	$\text{Jkg}^{-1}$	Latent heat of fusion
$\alpha, \beta$	$^{\circ}\text{C}^{-1}, \text{kg/g}$	Thermal expansion, haline contraction coefficients
$\gamma$	$\text{kg}^{2/3}\text{s}^{1/3}\text{m}^{-3}$	Entrainment parameter in (9)
$K_{\text{geo}}$	(no unit)	Geostrophic Ekman number
$x$	m	Distance downstream from shelf break
$W_s$	m	Initial plume width at shelf break
$\alpha_{\text{max}}$	(no unit)	Maximum topographic slope
$f$	$\text{s}^{-1}$	Coriolis parameter
$g$	$\text{ms}^{-2}$	Gravitational acceleration

TABLE 2. Experiments. The mixing fraction  $\phi = 0.33$ ; see section 3f for a discussion. For all experiments  $\delta\Phi = 0.01$  (see supplement section S1),  $T_i = -10^\circ\text{C}$ ,  $S_i = 4 \text{ g/kg}$ .

Experiment	Description	$U_1$	$T_1$	$S_1$	$Q$	$-\mathcal{F}$
		Sv	$^\circ\text{C}$	g/kg	TW	$\text{kts}^{-1}$
1	Fram Strait+BSO	4.75	3.40	35.00	115	180
2	Fram Strait+BSO high $Q$	4.75	3.40	35.00	153	180
3	Fram Strait+BSO various $Q$	4.75	3.40	35.00	87–195	180
4	Fram Strait+BSO various parameters	3.17–7.13	2.55–4.53	34.30–35.70	70–280	75–300
5	Fram Strait+BSO various $S_2$	4.75	3.40	35.00	115	180
6	Antarctic	26.0	0.50	34.84	300	240

## LIST OF FIGURES

- Fig. 1.** Upper two panels: Observations of temperature, salinity and normal geostrophic current across the Fram Strait and Barents Sea Opening. Modified from Klinger and Haine (2019) and based on results from Tsubouchi et al. (2012). Lower panel: Temperature and salinity data from Fram Strait in August 2002 (light gray) and from the Barents Sea Opening in August 2017 (dark gray; from the World Ocean Database, Boyer et al. 2018). . . . . 40
- Fig. 2.** Top: Schematic of the conceptual polar overturning model. The sign convention is that positive volume fluxes are towards the right. For realistic solutions  $\{U_2, U_3, U_i, u_s, u_i\} < 0$  and  $u_1 > 0$ , as the arrows show. The topographic bump at section A (nominally, the Fram Strait and Barents Sea Opening) is for illustrative purposes: the dashed line represents the Antarctic case. Bottom: Flow chart showing the model parameters, principles, and output variables. Table 1 defines the symbols. . . . . 41
- Fig. 3.** Schematic of the processes affecting OW properties. The Atlantic Water (AW) properties are specified. The Polar Water (PW) properties are freezing temperature and salinity less than the maximum value given by the dotted line tangent to the AW isopycnal. The ambient Water (aW) properties are a mixture of PW and AW determined by  $\phi$ . The Overflow Water (OW) properties are a mixture of aW and SW determined by entrainment  $\Phi$ . . . . . 42
- Fig. 4.** Results for experiment 1, with parameters appropriate for the Arctic (Fram Strait and Barents Sea Opening, BSO). The upper panel shows temperature/salinity properties, as in Fig. 3. Curved black contours are the density anomaly  $\rho(T, S) - 1000 \text{ kgm}^{-3}$  and the thick black line is the freezing temperature. The left (right) column of panels show mass, salt, and heat fluxes crossing section A (B) in Fig. 2. The individual terms in (S1) and (S2) are shown with the horizontal bars. The blue error bars indicate the range of possible solutions (see text). This solution is entrainment dominated with  $\Phi \approx 0.94$ , warm OW, and a weak shelf circulation. . . . . 43
- Fig. 5.** As Fig. 4, except for experiment 2. This solution has similar mass and salt fluxes to experiment 1 shown in Fig. 4, but weak entrainment ( $\Phi \approx 0.13$ ), strong shelf circulation, and cold OW. The total ocean heat loss flux,  $Q$  is 33% times larger than for experiment 1. Notice the heat flux abscissa limits differ from Fig. 4. . . . . 44
- Fig. 6.** Results for experiment 3 for the Arctic. The top panel shows the normalized volume fluxes  $U_2, U_3$ , and  $U_i$ . The middle panel shows the OW properties  $T_3$  and  $S_3$ . The bottom panel shows the entrainment  $\Phi$ . In each case, the abscissa is the normalized ocean heat loss flux  $Q$ . The solid and dashed vertical lines indicate experiments 1 and 2, shown in Figs. 4 and 5, respectively. The hatched regions indicate no solutions are possible because  $U_2 \neq 0$ ; see text for details. . . . . 45
- Fig. 7.** Tradeoff between entrainment  $\Phi$  and shelf salinity  $S_s$  for fixed OW flux. Strong (weak) entrainment implies weak (strong) shelf circulation  $u_s$  from (6). Results from experiments 1 and 2, including the range of possible solutions, are shown. The theory curve is from (12). . . . . 46
- Fig. 8.** Results for experiment 4 for the Arctic. Normalized distributions of  $U_2, U_3$ , and  $U_i$  against the forcing parameter  $\mathcal{N}^* = Q + L'\mathcal{F} + (1 - S_i/S_1) + c_p \rho_1 (S_i/S_1 - 1) T_1 U_1$  for many solutions with different parameters  $\{\mathcal{F}, Q, U_1, T_1, S_1\}$  (see Table 2). In each case, the distribution is taken of the solutions with entrainment closest to the mean entrainment, like the bars in Fig. 4. The solid and dashed vertical lines indicate experiments 1 and 2, shown in Figs. 4 and 5, respectively. The white curves show the results from experiment 3, as in Fig. 6, which are a subset of the results from experiment 4. There are 525199 valid solutions in experiment 4. . . . . 47

- Fig. 9.** As Fig. 4, except for experiment 6 for the Antarctic. . . . . 48
- Fig. 10.** Schematics of the four main solution modes: (a) Heat crisis for small  $Q$  (like experiment 1), (b) OW emergency for intermediate  $Q$  (like experiment 6 and the middle of experiment 3), (c) Salt crisis for large  $Q$  (like experiment 2), and (d) Entrainment emergency for fresh PW and/or aW (like the small PW salinity end of experiment 5). These main solutions are determined by the forcing, indicated by the ocean heat loss flux  $Q$  (Figs. 6 and 8), and by the aW salinity (Fig. S2). See also supplement Fig. S3. . . . . 49



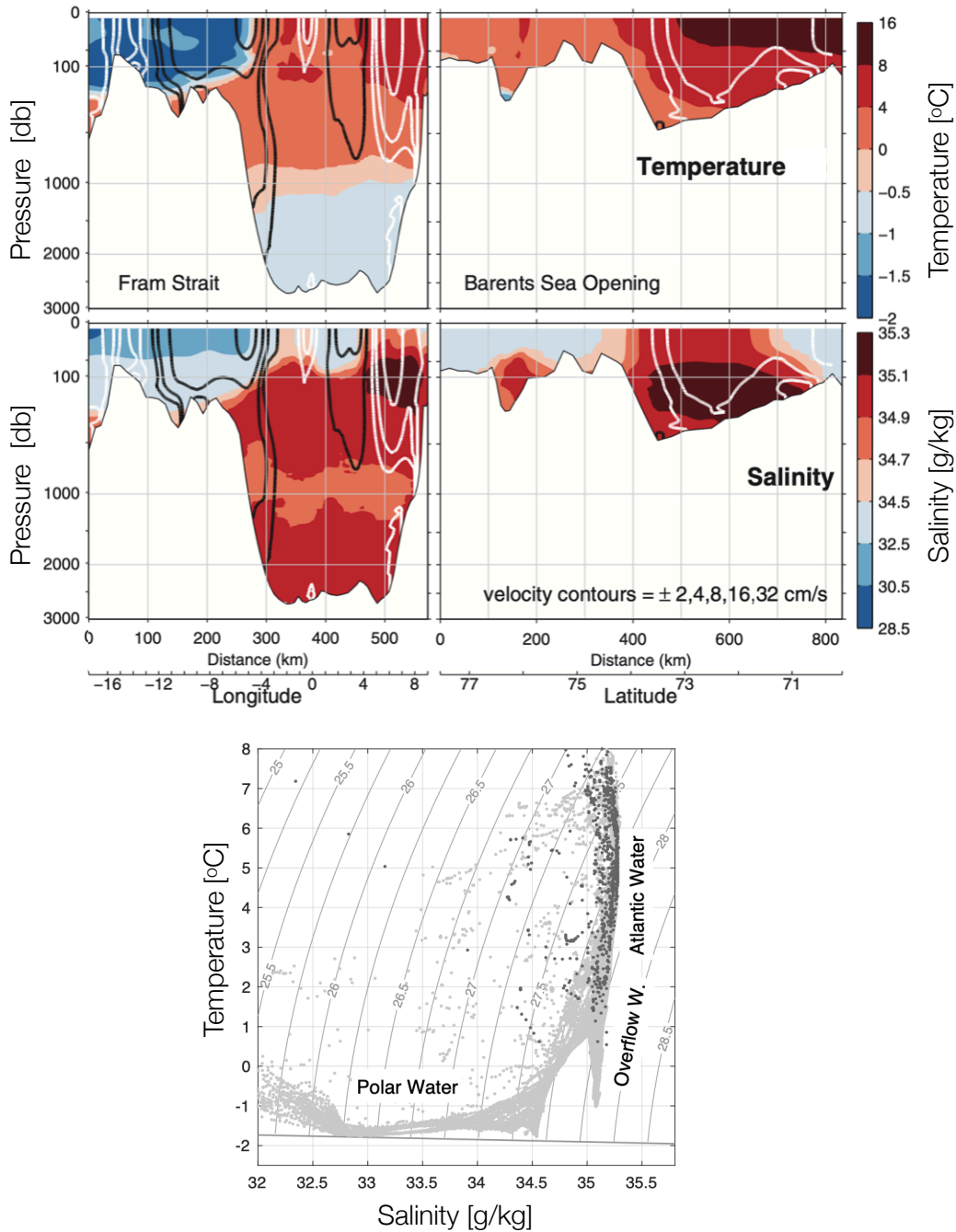


FIG. 1. Upper two panels: Observations of temperature, salinity and normal geostrophic current across the Fram Strait and Barents Sea Opening. Modified from Klinger and Haine (2019) and based on results from Tsubouchi et al. (2012). Lower panel: Temperature and salinity data from Fram Strait in August 2002 (light gray) and from the Barents Sea Opening in August 2017 (dark gray; from the World Ocean Database, Boyer et al. 2018).

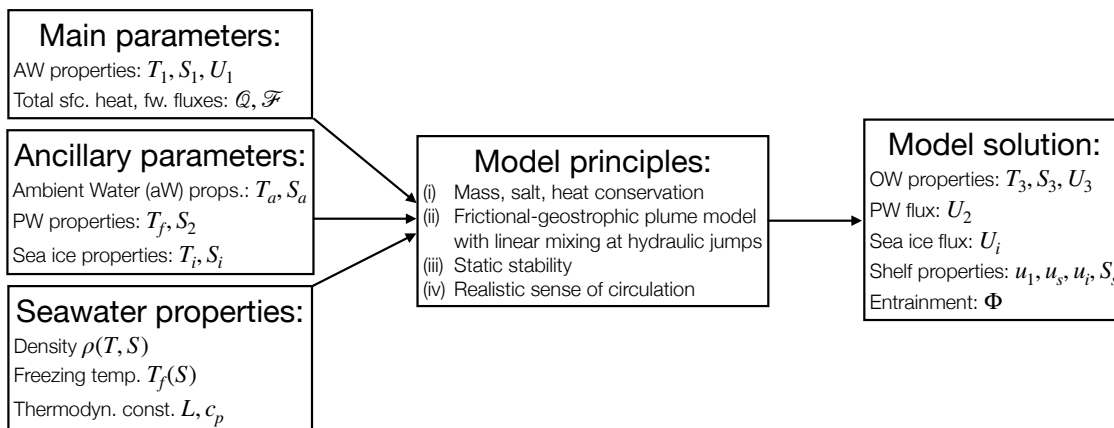
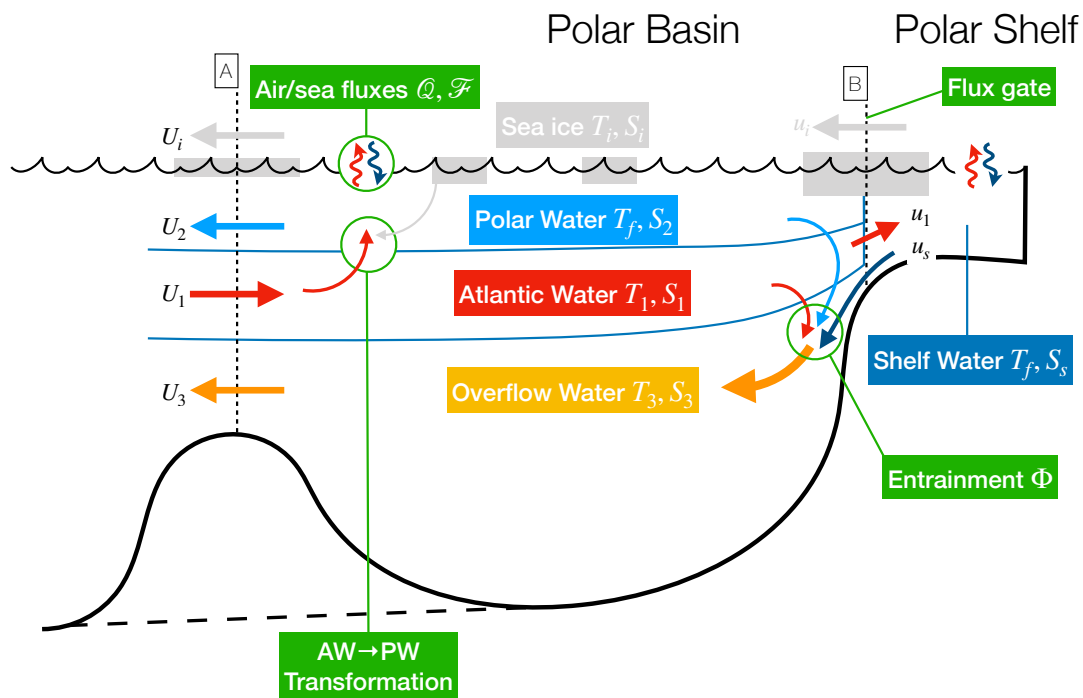


FIG. 2. Top: Schematic of the conceptual polar overturning model. The sign convention is that positive volume fluxes are towards the right. For realistic solutions  $\{U_2, U_3, U_i, u_s, u_i\} < 0$  and  $u_1 > 0$ , as the arrows show. The topographic bump at section A (nominally, the Fram Strait and Barents Sea Opening) is for illustrative purposes: the dashed line represents the Antarctic case. Bottom: Flow chart showing the model parameters, principles, and output variables. Table 1 defines the symbols.

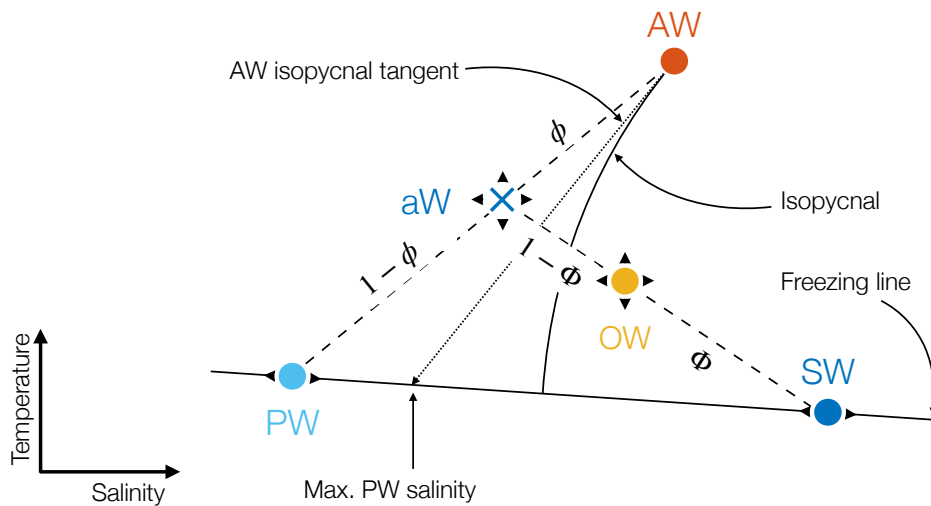


FIG. 3. Schematic of the processes affecting OW properties. The Atlantic Water (AW) properties are specified. The Polar Water (PW) properties are freezing temperature and salinity less than the maximum value given by the dotted line tangent to the AW isopycnal. The ambient Water (aW) properties are a mixture of PW and AW determined by  $\phi$ . The Overflow Water (OW) properties are a mixture of aW and SW determined by entrainment  $\Phi$ .

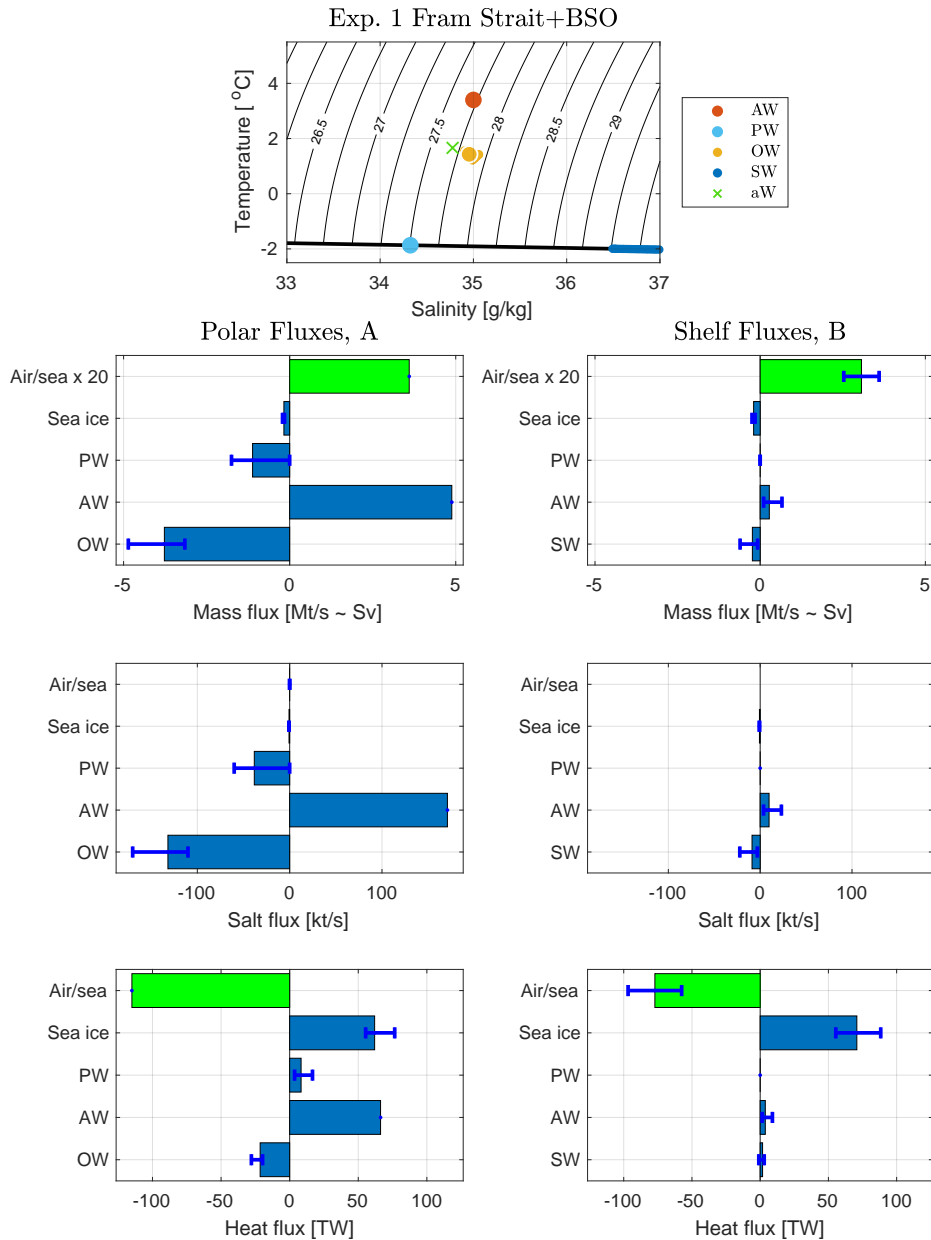


FIG. 4. Results for experiment 1, with parameters appropriate for the Arctic (Fram Strait and Barents Sea Opening, BSO). The upper panel shows temperature/salinity properties, as in Fig. 3. Curved black contours are the density anomaly  $\rho(T, S) - 1000 \text{ kg m}^{-3}$  and the thick black line is the freezing temperature. The left (right) column of panels show mass, salt, and heat fluxes crossing section A (B) in Fig. 2. The individual terms in (S1) and (S2) are shown with the horizontal bars. The blue error bars indicate the range of possible solutions (see text). This solution is entrainment dominated with  $\Phi \approx 0.94$ , warm OW, and a weak shelf circulation.

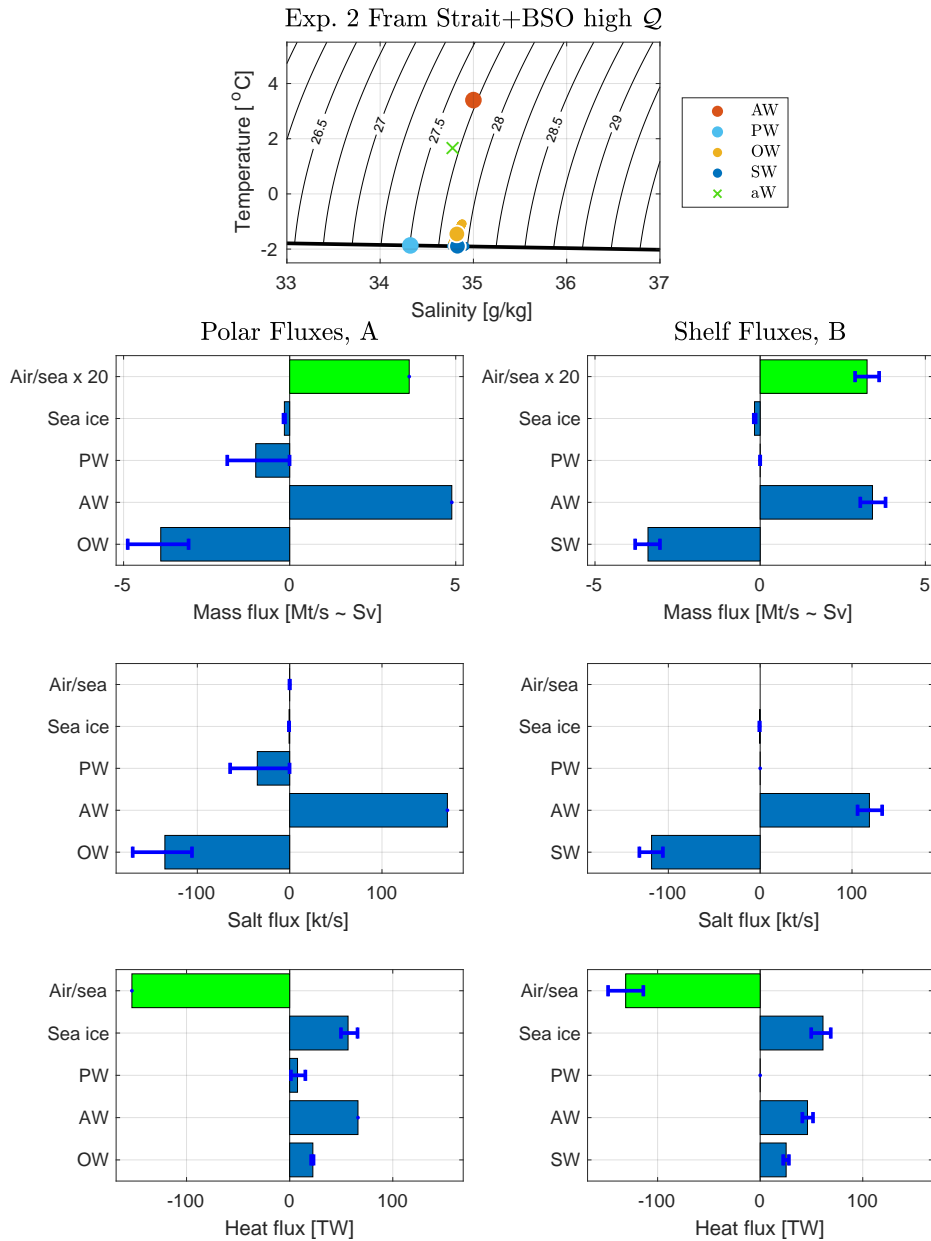


FIG. 5. As Fig. 4, except for experiment 2. This solution has similar mass and salt fluxes to experiment 1 shown in Fig. 4, but weak entrainment ( $\Phi \approx 0.13$ ), strong shelf circulation, and cold OW. The total ocean heat loss flux,  $Q$  is 33% times larger than for experiment 1. Notice the heat flux abscissa limits differ from Fig. 4.

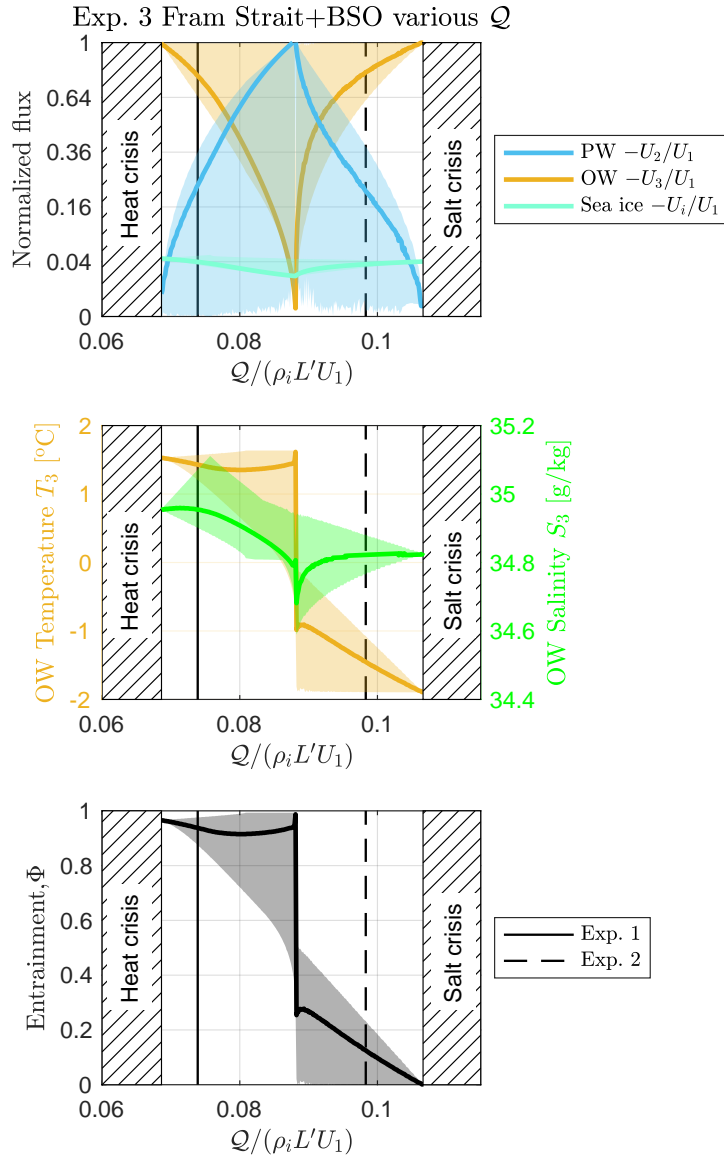


FIG. 6. Results for experiment 3 for the Arctic. The top panel shows the normalized volume fluxes  $U_2, U_3$ , and  $U_i$ . The middle panel shows the OW properties  $T_3$  and  $S_3$ . The bottom panel shows the entrainment  $\Phi$ . In each case, the abscissa is the normalized ocean heat loss flux  $Q$ . The solid and dashed vertical lines indicate experiments 1 and 2, shown in Figs. 4 and 5, respectively. The hatched regions indicate no solutions are possible because  $U_2 \neq 0$ ; see text for details.

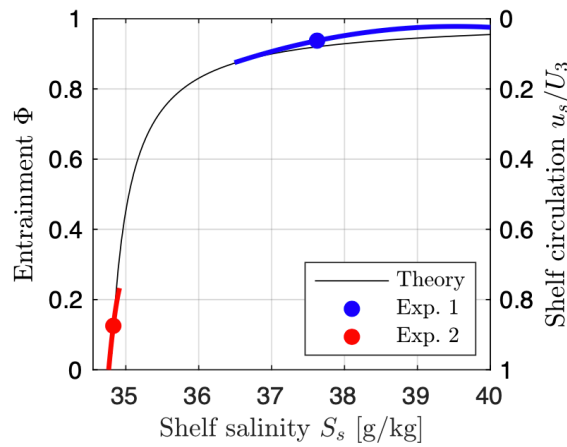


FIG. 7. Tradeoff between entrainment  $\Phi$  and shelf salinity  $S_s$  for fixed OW flux. Strong (weak) entrainment implies weak (strong) shelf circulation  $u_s$  from (6). Results from experiments 1 and 2, including the range of possible solutions, are shown. The theory curve is from (12).

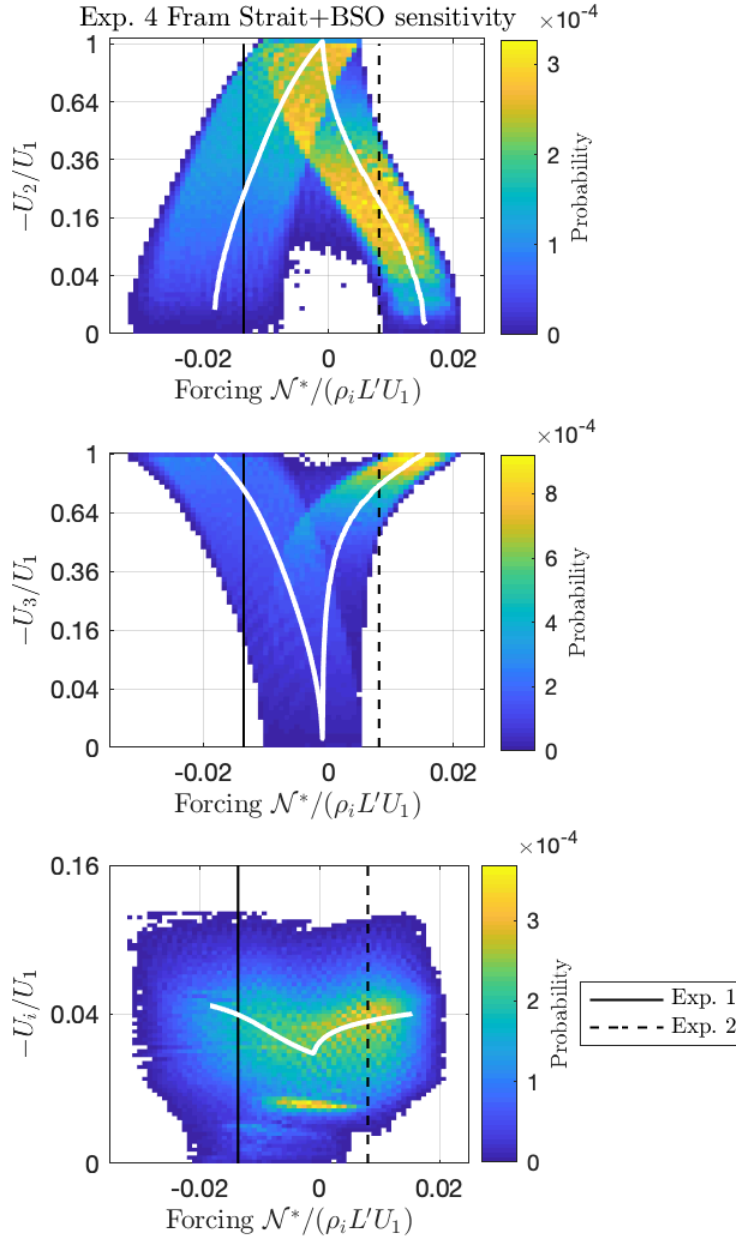


FIG. 8. Results for experiment 4 for the Arctic. Normalized distributions of  $U_2$ ,  $U_3$ , and  $U_i$  against the forcing parameter  $\mathcal{N}^* = Q + L'\mathcal{F} + (1 - S_i/S_1) + c_p\rho_1(S_i/S_1 - 1)T_1U_1$  for many solutions with different parameters  $\{\mathcal{F}, Q, U_1, T_1, S_1\}$  (see Table 2). In each case, the distribution is taken of the solutions with entrainment closest to the mean entrainment, like the bars in Fig. 4. The solid and dashed vertical lines indicate experiments 1 and 2, shown in Figs. 4 and 5, respectively. The white curves show the results from experiment 3, as in Fig. 6, which are a subset of the results from experiment 4. There are 525199 valid solutions in experiment 4.



Exp. 6 Antarctic

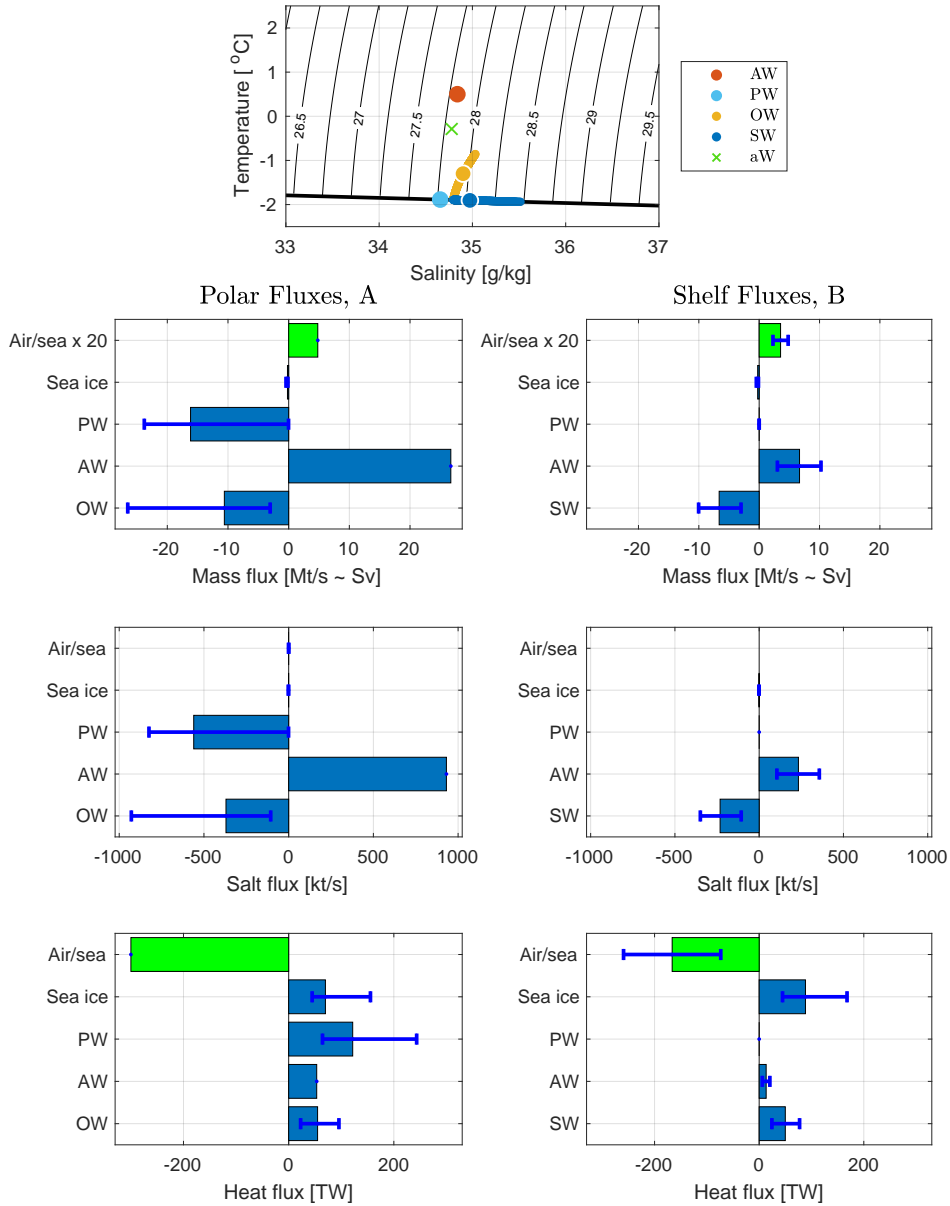


FIG. 9. As Fig. 4, except for experiment 6 for the Antarctic.

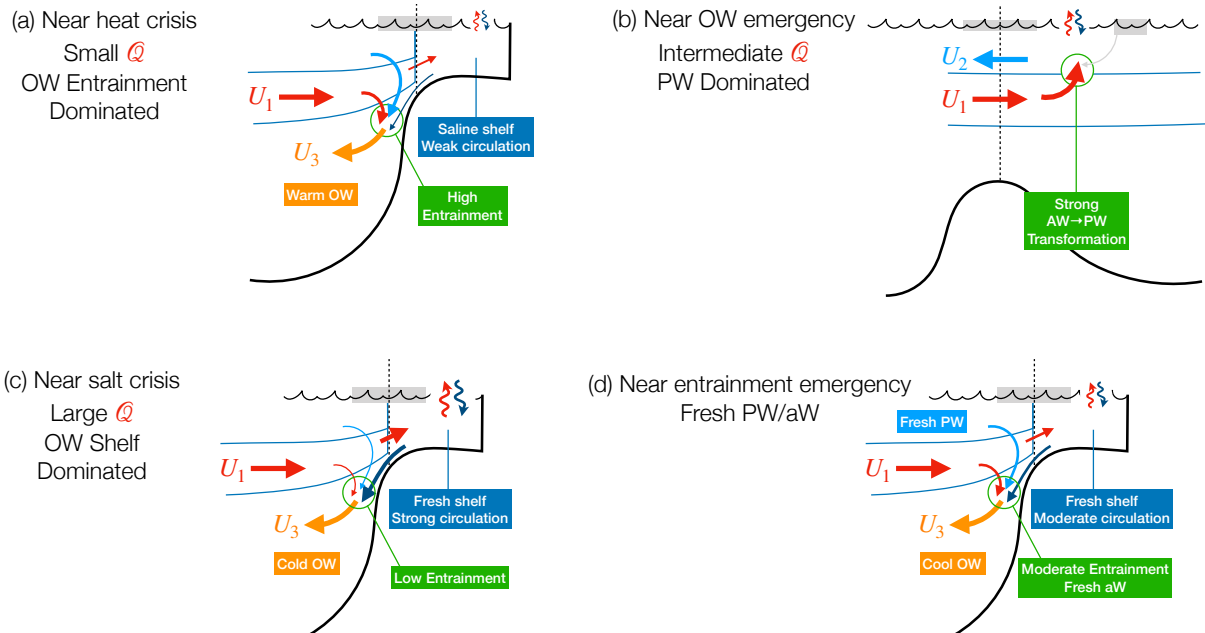


FIG. 10. Schematics of the four main solution modes: (a) Heat crisis for small  $Q$  (like experiment 1), (b) OW emergency for intermediate  $Q$  (like experiment 6 and the middle of experiment 3), (c) Salt crisis for large  $Q$  (like experiment 2), and (d) Entrainment emergency for fresh PW and/or aW (like the small PW salinity end of experiment 5). These main solutions are determined by the forcing, indicated by the ocean heat loss flux  $Q$  (Figs. 6 and 8), and by the aW salinity (Fig. S2). See also supplement Fig. S3.